HAL
open science

Arabidopsis thaliana 2,3-bisphosphoglycerate-independent phosphoglycerate mutase 2 activity requires serine 82 phosphorylation

Pauline Duminil, Marlène Davanture, Céline Oury, Edouard Boex-fontvieille, Guillaume Tcherkez, Michel Zivy, Michael Hodges, Nathalie Glab

To cite this version:

Pauline Duminil, Marlène Davanture, Céline Oury, Edouard Boex-fontvieille, Guillaume Tcherkez, et al.. Arabidopsis thaliana 2,3-bisphosphoglycerate-independent phosphoglycerate mutase 2 activity requires serine 82 phosphorylation. The Plant Journal, In press, pp.Early Access. 10.1111/tpj.15395 . hal-03294433

HAL Id: hal-03294433

https://hal.science/hal-03294433v1

Submitted on 21 Jul 2021

HAL is a multi-disciplinary open access archive for the deposit and dissemination of scientific research documents, whether they are published or not. The documents may come from teaching and research institutions in France or abroad, or from public or private research centers.

L'archive ouverte pluridisciplinaire **HAL**, est destinée au dépôt et à la diffusion de documents scientifiques de niveau recherche, publiés ou non, émanant des établissements d'enseignement et de recherche français ou étrangers, des laboratoires publics ou privés.

Arabidopsis thaliana 2,3-bisphosphoglycerate-independent phosphoglycerate mutase 2 activity requires serine 82 phosphorylation

Pauline DUMINIL[1], Marlène DAVANTURE[2], Céline OURY[1], Edouard BOEX-FONTVIEILLE[1], Guillaume TCHERKEZ[3,4], Michel ZIVY[2], Michael HODGES[1] and Nathalie GLAB[1]*

[1]Université Paris-Saclay, CNRS, INRAe, Univ Evry, Institute of Plant Sciences Paris-Saclay (IPS2), 91190 Gif sur Yvette, France

[2] Université Paris-Saclay, CNRS, INRAE, AgroParisTech, PAPPSO, GQE-Le Moulon, 91190 Gif-sur-Yvette, France

[3] Research School of Biology, ANU Joint College of Sciences, Australian National University, 2601, Canberra, ACT, Australia

[4] Institut de Recherche en Horticulture et Semences, Université d'Angers, INRAe, 42 rue Georges Morel, 49070 Beaucouzé, France

*Correspondence: nathalie.glab@universite-paris-saclay.fr

Running head: Phospho-S82 is an indicator of iPGAM activity

Key words: 2,3-bisphosphoglycerate-independent phosphoglycerate mutase, glycolysis, transient phosphorylation, catalytic mechanism, phosphopeptide, *Arabidopsis thaliana*

e-mail address of authors

Pauline DUMINIL: pauline.duminil@uni-goettingen.de

Marlène DAVANTURE: marlene.davanture@inrae.fr

Céline OURY: celine.oury@universite-paris-saclay.fr

Edouard BOEX-FONTVIEILLE: edouard.boex-fontvieille@interieur.gouv.fr

Guillaume TCHERKEZ: guillaume.tcherkez@anu.edu.au

Michel ZIVY: michel.zivy@inrae.fr

Michael HODGES: michael.hodges@cnrs.fr

Nathalie GLAB: nathalie.glab@universite-paris-saclay.fr

Summary

Phosphoglycerate mutases (PGAMs) catalyse the reversible isomerisation of 3-phosphoglycerate and 2-phosphoglycerate, a step of glycolysis. PGAMs can be sub-divided into 2,3-biphosphoglycerate dependent (dPGAM) and independent (iPGAM) enzymes. In plants, phosphoglycerate isomerisation is carried out by cytosolic iPGAM. Despite its crucial role in catabolism, little is known about post-translational modifications of plant iPGAM. In *Arabidopsis thaliana*, phosphoproteomics analyses have previously identified a iPGAM phosphopeptide where serine 82 is phosphorylated. Here, we show that this phosphopeptide is less abundant in dark-adapted compared to illuminated Arabidopsis leaves. *In silico* comparison of iPGAM protein sequences and 3D-structural modelling of *At*iPGAM2 based on non-plant iPGAM enzymes suggest a role for phosphorylated serine in the catalytic reaction mechanism. This is confirmed by the activity (or the lack thereof) of mutated recombinant Arabidopsis iPGAM2 forms, affected in different steps of the reaction mechanism. We thus propose that the occurrence of the S82-phosphopeptide reflects iPGAM2 steady-state catalysis. Based on this assumption, the metabolic consequences of a higher iPGAM activity in illuminated versus darkened leaves are discussed.

Introduction

Phosphoglycerate mutase (PGAM) catalyzes the reversible isomerization of 3-phosphoglycerate (3-PGA) and 2-phosphoglycerate (2-PGA), and it is involved in glycolysis and gluconeogenesis. There are two evolutionary unrelated PGAM groups, based on their requirement of a cofactor, 2,3-bisphosphoglycerate. Cofactor-dependent PGAM (dPGAM, E.C. 5.4.2.11) is present in vertebrates, some fungi and bacteria where it is often the only type of PGAM, like in humans (Fothergill-Gilmore and Watson, 1989). Cofactor-independent PGAM (iPGAM, E.C. 5.4.2.12) is found in higher plants, algae, some invertebrates including Nematodes, Trypanosomatideae, some fungi and bacteria (mainly Gram-positive) and requires a divalent cation for catalysis. These two groups of PGAMs show few similarities and can be distinguished by their protein sequence, their protein structure and their catalytic mechanism (Jedrzejas, 2000). Furthermore, iPGAM proteins can be classified into

two families according to their amino acid sequence and cation dependence: family 1 is composed of enzymes found in Trypanosomatideae and plants and use Mg^{2+}/Zn^{2+}, while family 2 members can be found in Prokaryotes and require Mn^{2+} to be active (Fuad *et al.*, 2011; Blackburn *et al.*, 2014). The 3D structure of family 1 iPGAM from the parasitic protozoans *Leishmania mexicana* (*Lm*iPGAM) and *Trypanosoma brucei* (*Tp*iPGAM), and family 2 enzymes from *Geobacillus stearothermophilus* (*Gs*iPGAM), *Staphylococcus aureus* (*Sai*PGAM) and *Bacillus anthracis* (*Ba*iPGAM) have been determined. Such crystallographic data revealed that the monomeric, globular enzyme is composed of two domains: phosphatase (domain A) which comprises the substrate binding site, and the transferase (domain B). The two domains are linked by a flexible junction necessary to allow conformational changes leading to either an open or a closed state required for catalysis (Jedrzejas *et al.*, 2000). Essential amino acids for catalysis have been identified and it was shown that phosphate group transfer during the isomerization reaction involved a transient phospho-serine (Jedrzejas *et al.*, 2000; Nukui *et al.*, 2007; Nowicki *et al.*, 2009; Mercaldi *et al.*, 2012; Roychowdhury *et al.*, 2015).

In plants, there has been a controversy as to whether both dPGAM and iPGAM exist and whether PGAM is located to both the cytosol and plastids. Pea (*Pisum sativum*) leaf chloroplasts do not contain any detectable PGAM activity (Stitt and Ap Rees, 1978). Contradictory observations have been reported in castor bean (*Ricinus communis*) endosperm: on the one hand, a very low PGAM activity was found in leucoplasts in addition to a high cytosolic PGAM activity (Miernyk and Dennis, 1982; Botha and Dennis, 1986) while on the other hand, only cytosolic iPGAM was found by Huang *et al.* (1993). To date, iPGAM purified from castor bean endosperm (Botha and Dennis, 1986), wheat germ (Smith and Hass, 1985) and maize seeds (Grana *et al.*, 1989) has been associated with a 60-74 kDa monomeric protein with a cofactor-independent activity and a Michaelis constant (K_m) for 3-PGA between 0.33 mM and 0.43 mM.

In *Arabidopsis thaliana*, TAIR and KEGG databases, along with several publications suggest the presence of several putative PGAM-encoding genes (Mazarei *et al.*, 2003; Andriotis *et al.*, 2010; Stein *et al.*, 2010). Amongst them, *At1g22170* was annotated as a dPGAM and shown to be localised to plastids; nevertheless, a mutant affected in that gene (*pglym1*) did not exhibit any phenotype and seed lipid content remained unaltered (Andriotis *et al.*, 2010). Two Arabidopsis genes, *At1g09780* and *At3g08590*, encoding 61 kDa

proteins sharing 90% identity and high similarities with other known higher plant iPGAMs were annotated *iPGAM1* and *iPGAM2*, respectively (Zhao and Assmann, 2011). They appear to have redundant functions since single *ipgam* mutants with a moderately reduced leaf iPGAM activity are indistinguishable from wild-type plants. However, *ipgam1 ipgam2* double mutants where leaf iPGAM activity is undetectable, displayed severely stunted growth, altered stomatal movements and an absence of pollen production thus leading to male sterility (Zhao and Assmann, 2011). In potato (*Solanum tuberosum*) lines where iPGAM activity had been reduced to 25% of the wild-type level using an anti-sense strategy, a slower growth leading to smaller plants and lower tuber yields were observed (Westram *et al.*, 2002).

Taken as a whole, genetics-based results point out the importance of iPGAM in plant development. Such an effect is expected considering its involvement in glycolysis, and the pivotal role of 3-PGA in plant metabolism. Glycolysis is a ubiquitous metabolic pathway occurring in the cytosol of all cell types where it can transform glucose to pyruvate, allowing the generation of reducing power and energy as NADH and ATP, respectively. The oxidation of pyruvate to acetyl-CoA can feed the mitochondrial tricarboxylic acid cycle (TCA cycle). It has been found that several glycolytic enzymes including iPGAM are attached to the cytosolic side of mitochondrial envelope (Giegé *et al.*, 2003). Glycolytic enzymes can be found also in plastids where they contribute to lipid metabolism but not all types of plastid contain PGAM (Plaxton, 1996; Givan, 1999). The fixation of atmospheric CO_2 and O_2 by ribulose-1,5-bisphosphate carboxylase/oxygenase (Rubisco) produces large amounts of 3-PGA used to fuel the Calvin cycle and starch biosynthesis in chloroplasts. Triose-phosphate molecules generated in chloroplasts from 3-PGA are transported to the cytosol *via* the triose-phosphate transporter (TPT) (for a review see Facchinelli and Weber, 2011) and used to synthesize sucrose, organic and amino acids as well as precursors for secondary metabolism and fatty acid biosynthesis. Interactions between metabolic pathways, such as the competition between triose phosphate utilization for sucrose synthesis versus catabolism, are tightly regulated and several glycolytic enzymes undergo post-translational redox modifications and/or protein phosphorylation while others have their activity modulated by metabolites (for a recent review see O'Leary and Plaxton, 2020). While a post-translational regulation of plant iPGAM activity has not been reported, the PhosPhAt

(http://phosphat.uni-hohenheim.de) and Athena (http://athena.proteomics.wzw.tum.de/) databases contain an *Arabidopsis thaliana* iPGAM phosphopeptide where serine 80 (S80) and serine 82 (S82) is phosphorylated in iPGAM1 and iPGAM2, respectively. Surprisingly, despite the crucial role of iPGAM, the potential impact of serine phosphorylation in modulating enzyme activity and participating in catalysis has never been examined.

Here, we looked at the role of serine 82 phosphorylation in Arabidopsis iPGAM2. Based on protein sequence comparisons and *in silico* structural modelling with non-plant iPGAM proteins, a strategy using recombinant Arabidopsis iPGAM2 and site-directed mutagenesis was adopted to test the hypothesis that S82 phosphorylation was part of the catalytic mechanism of plant iPGAMs. Since our *in vitro* studies suggest that the amount of detectable S82-phosphopeptide reflects iPGAM2 steady-state catalysis, the metabolic consequences of a higher *in planta* iPGAM activity in light-treated compared to light/dark-treated *Arabidopsis thaliana* rosette leaves were analyzed.

Results

*S82 of iPGAM2 is phosphorylated in Arabidopsis phosphoproteom*e

Phosphoproteomics analyses were carried out on Arabidopsis rosettes after either 4 h light or 4 h light followed by 2 h dark in a gas exchange system (and sampled by snap freezing with liquid nitrogen). A phosphopeptide associated with *At*iPGAM1 and *At*iPGAM2 was found, with the sequence AHGTAVGLPSEDDMGN(pS)EVGHNALGAGR, containing a phosphorylated serine at position 82 of *At*iPGAM2 (position 80 of *At*iPGAM1). Its abundance was significantly reduced by 30% in darkened leaves compared to illuminated leaves (Figure 1). Data mining in published phosphoproteomes and the literature showed that Arabidopsis iPGAM phosphorylation at this site is a common phenomenon (Table S1). In fact, many phosphoproteomics analyses have already identified this iPGAM phosphopeptide despite contrasting growth conditions: cell cultures (Carroll *et al.*, 2008; Ito *et al.*, 2009), cell suspensions (Nakagami *et al.*, 2010; Lin *et al.*, 2015), seedlings grown in liquid media (Wang *et al.*, 2013*a*,*b*; Hoehenwarter *et al.*, 2013; Xue *et al.*, 2013; Rayapuram *et al.*, 2014, 2018), *in vitro* seedlings (Lan *et al.*, 2012; Umezawa *et al.*, 2013; Yang *et al.*, 2013; Choudhary *et al.*, 2015), hydroponically grown plants (Zhang *et al.*, 2013), and adult plants grown in pots

(Roitinger *et al.*, 2015) (see Table S1). More recently, it has been identified in each of the 30 matching tissues from *Arabidopsis thaliana* (Col-0) of the Athena database.

Arabidopsis iPGAM structure and function

iPGAM catalysis involves a transitory phosphorylated serine residue to allow phosphate transfer from the C3 position of phosphoglycerate to the C2 position to form 2-phosphoglycerate. However, there is no information about the identity of the catalytic serine in iPGAM from plants. Protein sequence alignment of Arabidopsis iPGAM2 with iPGAM from *Trypanosoma brucei* and *Leshmania mexicana* (family 1) and *Staphylococcus aureus*, *Bacillus anthracis*, *Geobacillus stearothermophilus* (family 2) were carried out to identify a putative catalytic serine in the Arabidopsis enzyme (Figure S1). First, *At*iPGAM was found to share higher sequence identity with family 1 iPGAM proteins (57.8% with *T. brucei* and 56.3% with *L. mexicana*) than with family 2 proteins (35.9-37.5%). Second, sequence alignments clearly indicated that S82 of *At*iPGAM2 corresponded to S62 of *Sa*iPGAM and *Gs*iPGAM, S74 of *Tb*iPGAM and S75 of *Lm*iPGAM (Blackburn *et al.*, 2014), which have been demonstrated to undergo a transient phosphorylation as part of the catalytic reaction mechanism. Third, it was apparent that residues known to be involved in non-plant iPGAM catalysis (e.g. see Nowicki *et al.*, 2009) were conserved in the *At*iPGAM2 protein (Figure S1).

The relationship between conserved residues and *At*iPGAM function was further investigated using an *in-silico* predicted 3D structural model of *At*iPGAM2 constructed with SWISS MODEL (https://swissmodel.expasy.org/) and identified in the Swiss Model Repository (SMR; https://swissmodel.expasy.org/repository), a database of annotated 3D protein structure models generated by the SWISS-MODEL homology-modelling pipeline (Bienert *et al.*, 2017). The SMR proposed 3 templates to model *At*iPGAM2 structure (see A0A384KAQ5 at the SMR database), 3nvl.1.A (*T. brucei*), 3igy.1.A (*L. mexicana*) and 5kgl.1.A (*C. elegans*) (Figure S2). Although *T. brucei* iPGAM gave a slightly better Qualitative Model Energy ANalysis (QMEAN) score, it was decided to use *L. mexicana* iPGAM as the template in this study since the structure had been solved to a 2Å resolution, and crystallized in the presence of 3-PGA and two divalent cations (here Co^{2+}) and therefore it was in the active closed conformation. It can be seen that *At*iPGAM2 secondary structure predictions based on the chosen template indicated conserved α-helix and β-sheet domains with few

differences (Figure 2a) and the *At*iPGAM2 3D-predicted structure allowed a clear identification of the phosphatase domain A composed of amino- and carboxy-termini regions connected via two inter-domain loops to the transferase domain B (Figure 2b). A focus on the active site provided information on conserved amino acids involved in the catalysis and how they interact with the substrate and divalent cations (Figure 2c). The model confirmed S82 of *At*iPGAM2 as the putative catalytic serine interacting with both 3-PGA and a cobalt cation (Figure 2c). It also indicated the roles of conserved catalytic residues including the interaction of D431, H435 and H505 with one of the two metal ions (Co1) (Figure S3a), the interaction of D29, S82, D472 and H473 with the other divalent cation (Co2) (Figure S3b), 3 H-bonds between 3-PGA and S82 and R207 (Figure S3c) and 14 salt bridges between 3-PGA and S82, H141, R171, R207, R214, R290, R287, K362, H365, H435, H473 and H502 (Figure S3d).

Thus, both the sequence comparison (Figure S1) and the 3D structure prediction of *At*iPGAM2 (Figure 2 and Figure S3) strongly suggested a central role for S82 in the catalytic mechanism of plant iPGAM. Therefore, it was decided to investigate this further by a site directed mutagenesis approach using recombinant *At*iPGAM2.

*Characterisation of recombinant At*iPGAM *kinetic parameters*

Recombinant His-tagged *At*iPGAM2 was produced in *E. coli* cells and purified from the soluble fraction using affinity chromatography (Figure S4). It was then used to measure *At*iPGAM2 activity with a coupled enzymatic assay (Figure S5) previously used to measure iPGAM activity in Arabidopsis leaf extracts (Zhao and Assmann, 2011). The calculation of *At*iPGAM kinetic parameters showed the K_m for 3-PGA was 0.467±0.032 mM. This value is similar to those reported for other plant iPGAM proteins; recombinant castor bean iPGAM (0.43 mM; Huang and Dennis, 1995), and iPGAM purified from either castor bean endosperm (0.33 mM and 0.4 mM; Botha and Dennis, 1986) or maize seed (0.324 mM; Grana *et al.*, 1989). Specific activity (k_{cat}) was found to be 51.3±3.5 s^{-1} with 3-PGA as substrate in the presence of 5 mM Mg^{2+}. The presence of an N-terminal His-tag did not appear to interfere with its correct functioning and therefore our recombinant *At*iPGAM2 was used to investigate the role of S82.

Significance of the phosphorylated S82-containing peptide

To confirm the hypothesis that S82 of *At*iPGAM was indeed required by the enzyme to carry out the isomerization reaction, it was decided to produce and purify recombinant AtiPGAM2 where S82 had been replaced either by alanine (*At*iPGAM2$_{S82A}$) or aspartate (*At*iPGAM2$_{S82D}$) (Figure S4). The 3-PGA-dependent activity was abolished in both cases (Figure S6), thus highlighting the cardinal role of S82 in the catalytic mechanism of *At*iPGAM2.

To demonstrate that S82 phosphorylation was associated with *At*iPGAM2 activity, the amount of S82-phosphopeptide was measured at varying substrate concentration using recombinant *At*iPGAM2$_{WT}$ (Figure 3). Importantly, even in the absence of 3-PGA, the phosphopeptide was identified, showing that *At*iPGAM2 produced from *E. coli* cells was phosphorylated and functional within the bacterium and that the phosphorylated serine residue was stable, at least to some extent, during protein purification. When recombinant *At*iPGAM2 was incubated for 10 min with either 2.5 mM, or 5 mM or 10 mM 3-PGA, there was a significant 3-PGA-dependent increase in the amount of detectable phosphopeptide. Accordingly, the level of the phosphopeptide was lower when 3-PGA-dependent *At*iPGAM2 activity was assayed in the absence of added Mg^{2+}, however it was still higher than in the absence of 3-PGA probably due to the presence of cation still bound to a fraction of the purified, desalted protein (Figure 3).

We then used our protein sequence alignment (Figure S1) and structural model of *At*iPGAM2 (Figure 2c and Figure S3) and chose two conserved amino acids known to participate in catalysis in non-plant PGAMs. Structural studies of iPGAM from other species have demonstrated that an aspartate residue found in the N-terminus region is involved in the phospho-transferase reaction. This aspartate residue located in domain A corresponded to D29 in *At*iPGAM2, as it aligned with D11/12 of family 2 iPGAMs, and D22/23 of *Tb*iPGAM and *Lm*iPGAM family 1 enzymes, respectively (Figure S1). It was expected that the absence of D29 would stabilize S82 phosphorylation in the absence of the transferase reaction. On the other hand, R290 in *At*iPGAM2 domain B was identified as being equivalent to R284 (*Tb*iPGAM), R285 (*Lm*iPGAM) and R260/R264 (*Sa*iPGAM/*Gs*iPGAM), an arginine residue required for 3-PGA binding to the active site *via* stabilization of negative charges carried by the phosphate group (Jedrzejas *et al.*, 2000; Nukui *et al.*, 2007; Nowicki *et al.*, 2009;

Mercaldi *et al.*, 2012; Roychowdhury *et al.*, 2015). Therefore, the absence of R290 was expected to inhibit the phosphorylation of S82.

Site-directed mutagenesis of *At*iPGAM2 was carried out to produce recombinant *At*iPGAM2$_{D29N}$ and *At*iPGAM2$_{R290L}$ proteins. These two proteins did not display 3-PGA dependent catalytic activity at all (Figure S6), thereby confirming the importance of D29 and R290 of *At*iPGAM2 in the reaction mechanism and their requirement for enzyme activity. To investigate further the significance of the *At*iPGAM2 S82-containing phosphopeptide, recombinant *At*iPGAM2$_{D29N}$ and *At*iPGAM2$_{R290L}$ proteins were incubated with or without 2.5 mM 3-PGA and the amount of phosphopeptide was estimated by liquid chromatography-tandem mass spectrometry (LC-MS/MS) (Figure 4). As predicted from the role of R290 in substrate binding, the phosphopeptide was barely detectable in *At*iPGAM2$_{R290L}$, and less abundant that in the WT protein (Figure 4). As expected, *At*iPGAM2$_{D29N}$ produced an increased amount of phosphopeptide (Figure 4) since the reaction was blocked, that is, the transferase activity could not take place in the absence of D29. The significant amount of phosphorylated S82 in the *At*iPGAM2$_{D29N}$ assay carried out in the absence of substrate indicated that the 3-PGA pool in *E. coli* cells was sufficient to allow the occurrence of some phosphatase activity before the protein was purified. These results show that the reaction mechanism of *At*iPGAM2 is similar to that described for non-plant iPGAM enzymes and involves a catalytic serine (S82 of *At*iPGAM2) that carries the phosphate during the isomerization reaction.

Metabolite profiling of light- and light/dark-treated Arabidopsis rosette leaves

Gas chromatography-mass spectrometry (GC-MS)-based metabolite profiling (Table 1 and Table S2) of the rosette leaves used for phosphoproteomics was carried out to examine possible changes in leaf metabolism between the 4 h light (light) and 4 h light followed by 2 h dark (light/dark) treatments carried out during the natural 8 h day period of our Arabidopsis plants. Organic acids (malate, citrate, and succinate) were significantly 1.5- to 3.5-fold lower in illuminated leaves compared to darkened leaves whereas several saturated fatty acids (lauric acid, palmitic acid and stearic acid) where found to be 2- to 5-fold higher (Table 1). Only a small non-significant 20% reduction in leaf pyruvate levels were measured between the light and the light/dark treated leaves (Table 1). Amino acid levels showed variable differences between the two treatments, some of them being significantly

lower in the light (Ala, Asp, Cys, GABA, Glu, Ile and Lys), while Pro was significantly higher (by 28%) in the light compared to darkened leaves. Other amino acids including aromatic and several branched-chain amino acids (Table 1) showed no significant changes (Gly, Leu, Met, Phe, Ser, Thr, Tyr and Val) (Table S2). Shikimate content did not change significantly between the two conditions (Table 1). Finally, in the light there was more glucose, glycolate and glycerate (Table S2).

Discussion

PGAM is of paramount importance for plant growth and development (Westram *et al.*, 2002; Zhao and Assmann, 2011) due to its involvement in glycolysis. The genome of the plant model *Arabidopsis thaliana* contains two iPGAM-encoding genes (*At1g09780* and *At3g08590*) producing two proteins iPGAM1 and iPGAM2 that share a sequence identity of 90% and redundant functions (Zhao and Assmann, 2011). Arabidopsis iPGAM1 and iPGAM2 share a common phosphopeptide containing a phosphorylated serine (at position 82 in *At*iPGAM2) identified in the literature, the PhosPhAt database (see Table S1), and during our phosphoproteomics analysis (Figure 1). In this work, we chose to determine the significance of iPGAM2 S82 phosphorylation.

iPGAM2 activity involves phosphorylation at serine 82

At a first glance, the phosphorylated serine (S82 of *A*tiPGAM2) could be interpreted as a post-translational modification regulating iPGAM activity, however this is not the case. It has been shown previously that non-plant iPGAM catalysis involves a transient phosphoserine carrying the phosphate group during the isomerization reaction (Jedrzejas *et al.*, 2000; Nukui *et al.*, 2007; Nowicki *et al.*, 2009; Mercaldi *et al.*, 2012; Roychowdhury *et al.*, 2015). Sequence alignments (Figure S1), and a structural model of *At*iPGAM2 (Figure 2 and Figure S3) indicated that S82 of *At*iPGAM2 corresponds to the catalytic phosphoserine. Although the transient catalytic phosphoserine was expected be too unstable to allow its detection using standard phosphoproteomics techniques, an associated phosphopeptide was indeed detectable (Table S1; Figure 1). The importance of S82 for *At*iPGAM activity was shown by the complete loss of PGA-dependent catalytic activity (Figure S6) when S82 was mutated to either alanine or aspartate. Phosphopeptide analyses of recombinant *At*iPGAM2

confirmed the involvement of S82 in phosphate transfer during the isomerization of 3-PGA to 2-PGA. First, the amount of detectable phosphopeptide was dependent on the amount of substrate (Figure 3). Second, the amount of detectable phosphopeptide was dependent on the phosphatase and transferase steps of catalysis. *At*iPGAM$_{R290L}$ affected in 3-PGA binding to the active site exhibited an extremely low amount of phosphopeptide with a phosphorylated-to-non-phosphorylated (OP/OH) ratio of only 0.08 (Figure 4). On the other hand, *At*iPGAM$_{D29N}$ showed an extremely high amount of phosphopeptide with an OP/OH ratio of almost 6 (Figure 4) since D29 is involved in phosphate group transfer from S82 to form 2-PGA in the 3-PGA-dependent reaction. Taken together, our results clearly show that the *At*iPGAM2 phosphopeptide is not related to a post-translational regulatory process but it is a consequence of the isomerization reaction. Due to the transient nature of S82 phosphorylation, the amount of the resulting phosphopeptide in steady-state catalysis is low. Interestingly, a comparative phosphoproteomics study of blast resistant and susceptible rice (*Oryza sativa*) cultivars in response to salicylic acid showed a positive correlation between iPGAM phosphopeptide amounts and iPGAM activity (Sun *et al.*, 2019).

In planta iPGAM phosphopeptide levels and leaf metabolism

As seen from Table S1, the *At*iPGAM1/2 S80/S82-phosphopeptide has been detected previously in Arabidopsis grown in continuous light, continuous dark, and treated to different stresses (including iron availability, N deprivation, dehydration, ABA, *flg22*, ionizing radiation) but no differential phosphorylation was reported. However, *At*iPGAM1/2 S80/S82-phosphopeptide levels were found to change (by a modest extent) between our light and darkened conditions (Figure 1). Thus the content in phosphorylated catalytic intermediate and therefore steady-state catalysis was associated with a slight but significant light/dark effect. This in turn suggests that 3-PGA concentration and thus isomerization to 2-PGA probably changed, possibly impacting glycolytic production of PEP and pyruvate.

In the light, CO_2 assimilation *via* Rubisco produces 3-PGA that is converted to triose-phosphates in chloroplasts. Some triose-phosphates are then transported to the cytosol and used to make sugars and precursors (e.g. PEP and pyruvate) of biosynthetic pathways producing amino acids, organic acids, fatty acids and isoprenoids (see Figure 5). Since chloroplasts do not contain a complete glycolytic pathway as they lack iPGAM (Stitt and ap

Rees, 1978) and enolase (Prabhakar *et al*., 2009; Fukayama *et al*., 2015) they cannot produce PEP and pyruvate directly from triose-phosphates and so they are imported from the cytosol *via* plastid transporters (Streatfield *et al.*, 1999; Lee *et al*., 2017). In the chloroplast, PEP is required for the biosynthesis of aromatic amino acids (Tyr, Trp, Phe) (Maeda and Dudareva, 2012) while pyruvate is used for the biosynthesis of isoprenoids, branched-chain amino acids and saturated fatty acids (Ohlorgge and Jawarski, 1997; Pulido et al., 2012; Xing and Last, 2017). Interestingly, chloroplastic saturated fatty acid and isoprenoid biosynthetic pathways are more active in the light compared to the dark. PEP also provides OAA/malate (*via* the anaplerotic function of PEP carboxylase) and pyruvate also provides acetyl-CoA (*via* pyruvate dehydrogenase, PDH) to the TCA cycle in mitochondria. In the light, it is believed that the TCA cycle is slowed down and can operate as two disconnected pathways and not as a cycle (see Sweetlove *et al*., 2010; Tcherkez *et al*., 2012). Indeed, mitochondrial PDH activity is reduced by a post-translational phosphorylation mechanism and product inhibition (Tovar-Méndez *et al*., 2003) and TCA cycle decarboxylation reactions are strongly reduced in the light when compared to the dark (Tcherkez *et al.*, 2008). Therefore, it would be important to maintain the activity of the lower end of cytosolic glycolysis in the light and in the dark to provide PEP and pyruvate for these essential metabolic pathways (see Figure 5). In that context, the activity of iPGAM is important both in light (biosynthesis of PEP which is partly transported to the chloroplast) and in the dark (catabolic activity driven by mitochondrial PDH and the TCA cycle). As such, the change in relative phosphopeptide content (Figure 1) which is accompanied by changes in metabolites (Table 1) could reflect either a decrease in the amount of cytosolic 3-PGA in the dark, and/or a quantitative change in the glycolytic flux. It has been shown that triose-phosphate and 3-PGA levels decrease rapidly when leaves are transferred from light to the dark (Arrivault *et al*., 2009; Voll *et al*., 2009). Under our experimental conditions, darkening was accompanied by a decrease in chloroplastic saturated fatty acids and an increase in TCA cycle organic acids while several branched-chain and aromatic amino acid levels remained unaffected (Table 1, see also Figure 5). Thus, it is also possible that iPGAM activity decreased in darkened leaves as a consequence of a lower demand for glycolytic precursors to fuel metabolic processes occurring in the dark. It is difficult to compare metabolite data obtained from different plant species grown in different light and nutrient conditions. In this work, light versus a light/dark treatment during the day period was used and whole rosettes

were sampled. Published data often refer to diurnal changes in metabolite levels of a leaf at a specific developmental stage. When compared to the metabolite changes reported in Tables 1 and S2, higher amounts of certain organic acids associated with the TCA cycle were found in the day compared to the night in tobacco (*Nicotiana tabacum*) (e.g. Schieble *et al.,* 2000; Voll *et al*., 2009). In potato, citrate was lower, malate was higher and fumarate was unchanged between day and night (Urbanczyk-Wochniak *et al*., 2005). That said, when light-treated Arabidopsis rosettes were darkened for 15 min a number of metabolite changes were similar to those observed in our conditions (Tables 1 and S2). Indeed, citrate, malate, and succinate were all lower in the light compared to after the dark treatment, and shikimate did not change (Arrivault *et al*., 2009). Perhaps such changes in organic acid levels between our light- and light/dark-treated plants (Table 1) could be interpreted as a less active TCA cycle functioning in the dark. In our study, there was a significant decrease in several saturated fatty acids during the 2 h dark period (Table 1). Such an observation could be expected since fatty acid biosynthesis is known to be stimulated in the light (Browse *et al.*, 1981) due to activation of acetyl-CoA carboxylase activity by thioredoxin (Sasaki *et al.*, 1997) and light-induced changes in pH and Mg^{2+} levels in the chloroplast stroma. Branched-chain and aromatic amino acid levels that are dependent on either PEP or pyruvate in chloroplasts were not affected by the dark period after the light treatment except for isoleucine (Table 1). These pathways appear to be mainly regulated by allosteric inhibition of key enzymes (Maeda and Dudareva, 2012; Xing and Last, 2017).

Conclusions and perspectives

Taken as a whole, our results show that the catalytic mechanism of *At*iPGAM2 involves the transient phosphorylation of S82. Under the assumption that the content in S82-phosphopeptide reflects steady-state catalysis, *in planta* iPGAM activity would be higher in the light than in the dark. Future studies are warranted to provide more insights into the possible role of iPGAM in the regulation of metabolism, for example using ^{13}C-labelled 3-PGA to follow its conversion to 2-PGA *in planta* under contrasting light conditions. Also, in the mechanism of phosphotransfer catalyzed by iPGAM, uncertainty remains as to whether it is accompanied by a $^{12}C/^{13}C$ or $^{16}O/^{18}O$ isotope effect. Typically, the abstraction of the phosphate group from C-3 of phosphoglycerate or addition of the phosphate group onto C-2 of glycerate could discriminate against ^{13}C and/or ^{18}O. If so, it would affect the isotope

natural abundance in metabolites. Future studies will take advantage of isotopic compound-specific analyses to examine these aspects.

Experimental procedures

Plant material

Arabidopsis thaliana ecotype Columbia (Col-0) seeds were sown and germinated on soil for at least one week before plantlets were transplanted to individual pots for growth in controlled rooms under short-day conditions with an 8 h light regime of 100 µmol photons.m^{-2}.s^{-1} and 16 h dark, 20 °C day/18 °C night and 65 % humidity. Phosphoproteome and GC-MS analyses were carried out on Arabidopsis rosettes placed in a home-made cuvette system to measure photosynthetic activities and sampled by spraying with liquid nitrogen after either 4 h in a photosynthetic steady-state under 250 µmol photons.m^{-2}.s^{-1} of photosynthetically active radiation and 10 % blue light (light-treated) or after 2 h in darkness following the 4 h light-treatment (light/dark-treated) as described in Boex-Fontvieille *et al.* (2014).

Plasmid constructions and site-directed mutagenesis

Cloning of wild-type, S82A and S82D mutated *AtiPGAM2* open reading frame (ORF) cDNA into pET16b was performed using the Gibson assembly-based method (Gibson *et al.*, 2009). For pET16b-*AtiPGAM2*$_{WT}$, two PCR amplified fragments were assembled, one corresponding to the pET16b backbone using primers pET16b-fw and pET16b-rev and native pET16b as template and the other to generate the *AtiPGAM2* ORF using primers iPGAM2-fw16b and iPGAM2-rev16b and *AtiPGAM2* ORF cDNA in pUNI51 as template obtained from the Arabidopsis Biological Resource Center as clone U10048 (Yamada *et al.*, 2003). For pET16b-*AtiPGAM2*$_{S82A}$ and pET16b-*AtiPGAM2*$_{S82D}$, the same strategy was applied except that mutated *AtiPGAM2* ORFs were obtained through the assembly of two PCR amplified fragments each obtained with the following primer combinations: (i) iPGAM2-fw16b and iPGAM2S82Arev and (ii) iPGAM2S82Afwd and iPGAM2-rev16b for *AtiPGAM2*$_{S82A}$ and (i) iPGAM2-fw16b and iPGAM2S82Drev and (ii) iPGAM2S82Dfwd and iPGAM2-rev16b for *AtiPGAM2*$_{S82D}$. To obtain pET16b-*AtiPGAM2*$_{D29N}$ and pET16b-*AtiPGAM2*$_{R290L}$, the previously described pET16b-*AtiPGAM2*$_{WT}$ was used as a template for site-directed mutagenesis using

the QuikChange Lightning Site-Directed Mutagenesis Kit (Agilent, Santa Clara, CA, United States) and primer combinations [563PRO+564TER] and [565PRO+566TER], respectively. All primer sequences are given in Table S3.

Purification of recombinant proteins

E. coli BL21 (DE3) cells containing either pET16b-*AtiPGAM2*$_{WT}$, pET16b-*AtiPGAM2*$_{D29N}$, pET16b-*AtiPGAM2*$_{S82A}$, pET16b-*AtiPGAM2*$_{S82D}$ or pET16b-*AtiPGAM2*$_{R290L}$ were grown in 400 mL of Luria-Bertani broth supplemented with ampicillin (50 mg.L^{-1}) at 37 °C until a OD_{600nm} of 0.8 was reached then *AtiPGAM2* expression was induced by the addition of isopropyl-β-1-D-thiogalactopyranoside (IPTG) 500 µM final concentration. After an overnight culture period at 20 °C, cells were centrifuged and resuspended in lysis buffer (3 mL for a 200 mL culture pellet) containing Tris-HCl 50 mM pH 7.5, NaCl 300 mM, imidazole 5 mM and a tablet of protease inhibitor (Complete Mini, EDTA-free, Roche Applied Science, Penzberg, Upper Bavaria, Germany) and broken by 3 repeated passes through a French press at 3.5 MPa. After a 30 min centrifugation at 4 °C and 27 000 g, recombinant proteins were purified on His-Select nickel affinity resin (P6611, Sigma-Aldrich, Saint-Louis, MO, United States) according to the manufacturer's "batch" protocol. Washing and elution were performed with modified lysis buffer containing 20 mM and 250 mM imidazole, respectively. Eluate was desalted using PD-10 filtration columns (GE Healthcare, Chicago, IL, United States) previously equilibrated with Tris-HCl 50 mM at pH 7.5 following the manufacturer's instructions. Protein concentrations were determined using the Pierce™ Coomassie Plus Assay Reagent (B6916, Sigma-Aldrich) and bovine serum albumin (A4503, Sigma-Aldrich) as the protein standard.

Enzymatic assay

iPGAM activity measurements were carried out at 30 °C using a Varian Cary 50 UV-Vis spectrophotometer (Agilent) at 340 nm, with 2.5 µg of recombinant protein in a 1 mL final volume containing Tris-HCl 30 mM pH 7.5, KCl 20 mM, $MgSO_4$ 5 mM, 3-PGA (0-10 mM), and 2.5 U each of enolase (E6126, Sigma-Aldrich; EC 4.2.1.11), pyruvate kinase (P7768, Sigma-Aldrich; EC 2.7.1.40), and lactate dehydrogenase (L2518 Sigma-Aldrich; EC 1.1.1.27) according to the coupled reaction described by Zhang *et al.* (2004) (see Figure S5). Kinetic

parameters were calculated using the "Kinetic Enzyme Wizard" of Sigma-Plot (Systat Software Inc., San Jose, CA, United States).

iPGAM2 phosphopeptide analyses

Recombinant iPGAM2 proteins (2.5 µg) were incubated at 30 °C with selected 3-PGA concentrations during 10 min in a 20 µL reaction buffer Tris-HCl 30 mM pH 7.5, KCl 20 mM, and $MgSO_4$ 5 mM. To test the effect of Mg^{2+}, iPGAM2 was also incubated in the absence of added cation in the presence of 2.5 mM 3-PGA. The reaction was stopped by the addition of Laemmli buffer 4X (Tris-HCl 240 mM pH 6.8, SDS 8 % (v/v), glycerol 40 % (v/v), bromophenol blue 0.04 % (w/v), β-mercaptoethanol 10 % (v/v)). Proteins were separated according to their molecular mass by SDS-PAGE (10 % acrylamide) (Laemmli, 1970). The protein band corresponding to iPGAM (61 kDa) was cut from the SDS-PAGE gel for phosphopeptide analysis according to Hummel *et al.* (2015). Phosphoproteome experiments carried out using proteins extracted from rosettes of either light- or light/dark-treated *Arabidopsis thaliana* plants have been previously described in Boex-Fontvieille *et al.* (2014).

GC-MS-based metabolite profiling

Metabolite profiling and data analyses were performed as described in Bathellier *et al.* (2009). Briefly, 20 mg of leaf powder from lyophilized leaf rosette samples was extracted with 2 mL methanol:water (70:30 v/v) to which ribitol 100 µM was added as an internal standard. Supernatants used for GC-MS (Pegasus III system; Leco, France) analyses were chemically derivatized with methoxyamine and MSTFA in pyridine.

In silico *analyses*

3D structural models of *At*iPGAM2 were made using either SWISS MODEL (https://swissmodel.expasy.org/) or identified in the Swiss Model Repository (SMR; https://swissmodel.expasy.org/repository). Multiple sequence alignment of iPGAM proteins was performed using Clustal Omega (1.2.4).

Data statement

The complete metabolomics data sets are not available in a public repository but they are available on request to michael.hodges@cnrs.fr

Acknowledgements

This work was supported by a public grant overseen by the French National Research Agency (ANR) as part of the "Investissement d'Avenir" programme, through the "Lidex-3P" project and a French State Grant (ANR-10-LABX-0040-SPS) funded by the IDEX Paris-Saclay. This work was also supported by the ANR-14-CE19-0015 grant Regul3P awarded to MH. PD was supported by a PhD grant from the French Ministry of Higher Education and Research. We would like to thank Samuel Mainguet, Julie Capitanio and Julie Mignon for their contributions to some of the experiments and Jean Vidal for his help with the manuscript. Authors declare that they have no conflicts of interest.

Supporting figures

Figure S1: Protein sequence alignments between *At*iPGAM2 and non-plant iPGAMs with resolved 3D-structures.

Figure S2: 3D structure of templates used for *At*iPGAM2 structure prediction.

Figure S3: *At*iPGAM2 structure prediction: catalytic core details.

Figure S4: Purification of *At*iPGAM2$_{WT}$, *At*iPGAM2$_{S82A}$, *At*iPGAM2$_{S82D}$, *At*iPGAM2$_{D29N}$ and *At*iPGAM2$_{R290L}$.

Figure S5: *At*iPGAM2 activity measurement with a coupled reaction.

Figure S6: 3-PGA-dependent iPGAM activity of recombinant wild-type and mutated *At*iPGAM2 proteins.

Supporting tables

Table S1: PhosPhAt 4.0 indexed phosphoproteomics experiments for the *At*iPGAM1/2 S82-containing phosphopeptide.

Table S2: GC-coupled with time-of-flight MS-determined metabolite levels of light- and light/dark-treated rosette leaves used for phosphoproteomics studies.

Table S3: Primers used for cloning and site-directed mutagenesis with their corresponding names, sequences, and Tm °C.

All data supporting the findings of this study are available within the paper and within its supporting information published online.

References

Andriotis VME, Kruger NJ, Pike MJ, Smith AM. (2010) Plastidial glycolysis in developing Arabidopsis embryos. New Phytologist **185**, 649–662. https://doi.org/10.1111/j.1469-8137.2009.03113.x

Arrivault S, Guenther M, Ivakov A, Feil R, Vosloh D, Van Dongen JT, Sulpice R, Stitt M. (2009) Use of reverse-phase liquid chromatography, linked to tandem mass spectrometry, to profile the Calvin cycle and other metabolic intermediates in Arabidopsis rosettes at different carbon dioxide concentrations. Plant Journal **59**, 826–839. https://doi.org/10.1111/j.1365-313X.2009.03902.x

Bathellier C, Tcherkez G, Mauve C, Bligny R, Gout E, Ghashghaie J. (2009) On the resilience of nitrogen assimilation by intact roots under starvation, as revealed by isotopic and metabolomic techniques. Rapid Communications in Mass Spectrometry **23**, 2847-2856. https://doi.org/10.1002/rcm.4198

Bienert S, Waterhouse A, de Beer TAP, Tauriello G, Studer G, Bordoli L, Schwede T. (2017) The SWISS-MODEL repository-new features and functionality. Nucleic Acids Research **45**, 313–319. https://doi.org/10.1093/nar/gkw1132

Blackburn EA, Fuad FAA, Morgan HP, Nowicki MW, Wear MA, Michels PAM, Fothergill-Gilmore LA, Walkinshaw MD. (2014) Trypanosomatid phosphoglycerate mutases have multiple conformational and oligomeric states. Biochemical and Biophysical Research Communications **450**, 936–941. https://doi.org/10.1016/j.bbrc.2014.06.113

Boex-Fontvieille E, Davanture M, Jossier M, Zivy M, Hodges M, Tcherkez G. (2014) Photosynthetic activity influences cellulose biosynthesis and phosphorylation of proteins involved therein in Arabidopsis leaves. Journal of Experimental Botany **65**, 4997–5010. https://doi.org/10.1093/jxb/eru268

Botha FC, Dennis DT. (1986) Isozymes of phosphoglyceromutase from the developing endosperm of *Ricinus communis*: Isolation and kinetic properties. Archives of Biochemistry and Biophysics **245**, 96–103. https://doi.org/10.1016/0003-9861(86)90193-1

Browse J, Roughan PG, Slack CR. (1981) Light control of fatty acid synthesis and diurnal fluctuations of fatty acid composition in leaves. The Biochemical Journal **196**, 347–354. https://doi.org/10.1042/bj1960347

Carroll AJ, Heazlewood JL, Ito J, Millar AH. (2008) Analysis of the Arabidopsis cytosolic ribosome proteome provides detailed insights into its components and their post-translational modification. Molecular and Cellular Proteomics **7**, 347–369. https://doi.org/10.1074/mcp.M700052-MCP200

Choudhary MK, Nomura Y, Wang L, Nakagami H, Somers DE. (2015) Quantitative circadian phosphoproteomic analysis of Arabidopsis reveals extensive clock control of key components in physiological, metabolic, and signaling pathways. Molecular and Cellular Proteomics **14**, 2243–2260. https://doi.org/10.1074/mcp.M114.047183

Facchinelli F, Weber APM. (2011) The metabolite transporters of the plastid envelope: an update. Frontiers in Plant Science **2**, 50. https://doi.org/10.3389/fpls.2011.00050

Fothergill-Gilmore LA, Watson HC. (1989) The phosphoglycerate mutases. Advances in Enzymology and Related Areas of Molecular Biology **62**, 227–313. https://doi.org/10.1002/9780470123089.ch6

Fuad FAA, Fothergill-Gilmore LA, Nowicki MW, Eades LJ, Morgan HP, McNae IW, Michels PAM, Walkinshaw MD. (2011) Phosphoglycerate mutase from *Trypanosoma brucei* is hyperactivated by cobalt *in vitro*, but not *in vivo*. Metallomics : Integrated Biometal Science **3**, 1310–1317. https://doi.org/10.1039/c1mt00119a

Fukayama H, Masumoto C, Taniguchi Y, Baba-Kasai A, Katoh Y, Ohkawa H, Miyao M. (2015) Characterization and expression analyses of two plastidic enolase genes in rice. Bioscience, Biotechnology and Biochemistry **79**, 402–409. https://doi.org/10.1080/09168451.2014.980219

Gibson DG, Young L, Chuang R-Y, Venter JC, Hutchison CA 3rd, Smith HO. (2009) Enzymatic assembly of DNA molecules up to several hundred kilobases. Nature Methods **6**, 343–345. https://doi.org/10.1038/nmeth.1318

Giegé P, Heazlewood JL, Roessner-Tunali U, Harvey Millar A, Fernie AR, Leaver CJ, Sweetlove LJ. (2003) Enzymes of glycolysis are functionally associated with the mitochondrion in Arabidopsis cells. Plant Cell **15**, 2140–2151. https://doi.org/10.1105/tpc.012500

Givan C V. (1999) Evolving concepts in plant glycolysis: two centuries of progress. Biological Reviews **74**, 277–309. https://doi.org/10.1111/j.1469-185X.1999.tb00188.x

Grana X, Urena J, Ludevid D, Carreras J, Climent F. (1989) Purification, characterization and immunological properties of 2,3-bisphosphoglycerate-independent phosphoglycerate

mutase from maize (*Zea mays*) seeds. European Journal of Biochemistry **186**, 149–153. https://doi.org/10.1111/j.1432-1033.1989.tb15189.x

Hoehenwarter W, Thomas M, Nukarinen E, Egelhofer V, Röhrig H, Weckwerth W, Conrath U, Beckers GJM. (2013) Identification of novel *in vivo* MAP kinase substrates in *Arabidopsis thaliana* through use of tandem metal oxide affinity chromatography. Molecular and Cellular Proteomics **12**, 369–380. https://doi.org/10.1074/mcp.M112.020560

Huang Y, Blakeley SD, McAleese SM, Fothergill-Gilmore LA, Dennis DT. (1993) Higher-plant cofactor-independent phosphoglyceromutase: purification, molecular characterization and expression. Plant Molecular Biology **23**, 1039–1053. https://doi.org/10.1007/BF00021818

Huang Y, Dennis DT. (1995) Histidine residues 139, 363 and 500 are essential for catalytic activity of cofactor-independent phosphoglyceromutase from developing endosperm of the castor plant. European Journal of Biochemistry **229**, 395–402. https://doi.org/10.1111/j.1432-1033.1995.tb20480.x

Hummel M, Dobrenel T, Cordewener J, Davanture M, Meyer C, Smeekens S, Bailey-Serres J, America T, Hanson J. (2015) Proteomic LC–MS analysis of Arabidopsis cytosolic ribosomes: Identification of ribosomal protein paralogs and re-annotation of the ribosomal protein genes. Journal of Proteomics **128**, 436–449. https://doi.org/10.1016/j.jprot.2015.07.004

Ito J, Taylor NL, Castleden I, Weckwerth W, Millar AH, Heazlewood JL. (2009) A survey of the *Arabidopsis thaliana* mitochondrial phosphoproteome. Proteomics **9**, 4229–4240. https://doi.org/10.1002/pmic.200900064

Jedrzejas MJ. (2000) Structure, function, and evolution of phosphoglycerate mutases: Comparison with fructose-2,6-bisphosphatase, acid phosphatase, and alkaline phosphatase. Progress in Biophysics and Molecular Biology **73**, 263–287. https://doi.org/10.1016/S0079-6107(00)00007-9

Jedrzejas MJ, Chander M, Setlow P, Krishnasamy G. (2000) Mechanism of catalysis of the cofactor-independent phosphoglycerate mutase from *Bacillus stearothermophilus*: Crystal structure of the complex with 2-phosphoglycerate. Journal of Biological Chemistry **275**, 23146–23153. https://doi.org/10.1074/jbc.M002544200

Laemmli UK. (1970) Cleavage of structural proteins during the assembly of the head of bacteriophage T4. Nature **227**, 680–685. https://doi.org/10.1038/227680a0

Lan P, Li W, Wen T-N, Schmidt W. (2012) Quantitative phosphoproteome profiling of iron-deficient Arabidopsis roots. Plant Physiology **159**, 403–417. https://doi.org/10.1104/pp.112.193987

Lee EJ, Oh M, Hwang JU, Li-Beisson Y, Nishida I, Lee Y. (2017) Seed-specific overexpression of the pyruvate transporter BASS2 increases oil content in Arabidopsis seeds. Frontiers in Plant Science **8**, 1–10. https://doi.org/10.3389/fpls.2017.00194

Lin L-L, Hsu C-L, Hu C-W, Ko S-Y, Hsieh H-L, Huang H-C, Juan H-F. (2015) Integrating phosphoproteomics and bioinformatics to study brassinosteroid-regulated phosphorylation dynamics in Arabidopsis. BMC Genomics **16**, 533. https://doi.org/10.1186/s12864-015-1753-4

Maeda H, Dudareva N. (2012) The shikimate pathway and aromatic amino acid biosynthesis in plants. Annual Review of Plant Biology **63**, 73–105. https://doi.org/10.1146/annurev-arplant-042811-105439

Mazarei M, Lennon KA, Puthoff DP, Rodermel SR, Baum TJ. (2003) Expression of an Arabidopsis phosphoglycerate mutase homologue is localized to apical meristems, regulated by hormones, and induced by sedentary plant-parasitic nematodes. Plant Molecular Biology **53**, 513–530. https://doi.org/10.1023/B:PLAN.0000019062.80459.80

Mercaldi GF, Pereira HM, Cordeiro AT, Michels PAM, Thiemann OH. (2012) Structural role of the active-site metal in the conformation of *Trypanosoma brucei* phosphoglycerate mutase. The FEBS Journal **279**, 2012–2021. https://doi.org/10.1111/j.1742-4658.2012.08586.x

Miernyk JA, Dennis DT. (1982) Isozymes of the glycolytic enzymes in endosperm from developing castor oil seeds. Plant Physiology **69**, 825–828. https://doi.org/10.1104/pp.69.4.825

Nakagami H, Sugiyama N, Mochida K, Daudi A, Yoshida Y, Toyoda T, Tomita M, Ishihama Y, Shirasu K. (2010) Large-scale comparative phosphoproteomics identifies conserved phosphorylation sites in plants. Plant Physiology **153**, 1161–1174. https://doi.org/10.1104/pp.110.157347

Nowicki MW, Kuaprasert B, McNae IW, Morgan HP, Harding MM, Michels PAM, Fothergill-Gilmore LA, Walkinshaw MD. (2009) Crystal structures of *Leishmania mexicana* phosphoglycerate mutase suggest a one-metal mechanism and a new enzyme subclass. Journal of Molecular Biology **394**, 535–543. https://doi.org/10.1016/j.jmb.2009.09.041

Nukui M, Mello L V, Littlejohn JE, Setlow B, Setlow P, Kim K, Leighton T, Jedrzejas MJ. (2007) Structure and molecular mechanism of *Bacillus anthracis* cofactor-independent phosphoglycerate mutase: a crucial enzyme for spores and growing cells of Bacillus species. Biophysical Journal **92**, 977–988. https://doi.org/10.1529/biophysj.106.093872

Ohlrogge JB, Jaworski JG. (1997) Regulation of fatty acid synthesis. Annual Review of Plant Biology **48**, 109–136. https://doi.org/10.1146/annurev.arplant.48.1.109

O'Leary B, Plaxton WC. (2020) Multifaceted functions of post-translational enzyme modifications in the control of plant glycolysis. Current Opinion in Plant Biology **55**, 28–37. https://doi.org/10.1016/j.pbi.2020.01.009

Plaxton WC. (1996) The organization and regulation of plant glycolysis. Annual Review of Plant Physiology and Plant Molecular Biology **47**, 185–214. https://doi.org/10.1146/annurev.arplant.47.1.185

Prabhakar V, Löttgert T, Gigolashvili T, Bell K, Flügge U, Häusler RE. (2009) Molecular and functional characterization of the plastid-localized phosphoenolpyruvate enolase (ENO1) from *Arabidopsis thaliana*. FEBS Letters **583**, 983–991. https://doi.org/10.1016/j.febslet.2009.02.017

Pulido P, Perello C, Rodriguez-Concepcion M. (2012) New insights into plant Isoprenoid metabolism. Molecular Plant **5**, 964–967. https://doi.org/10.1093/mp/sss088

Rayapuram N, Bigeard J, Alhoraibi H, Bonhomme L, Hesse A-M, Vinh J, Hirt H, Pflieger D. (2018) Quantitative phosphoproteomic analysis reveals shared and specific targets of Arabidopsis mitogen-activated protein kinases (MAPKs) MPK3, MPK4, and MPK6. Molecular and Cellular Proteomics **17**, 61–80. https://doi.org/10.1074/mcp.RA117.000135

Rayapuram N, Bonhomme L, Bigeard J, Haddadou K, Przybylski C, Hirt H, Pflieger D. (2014) Identification of novel PAMP-triggered phosphorylation and dephosphorylation events in *Arabidopsis thaliana* by quantitative phosphoproteomic analysis. Journal of Proteome Research **13**, 2137–2151. https://doi.org/10.1021/pr401268v

Roitinger E, Hofer M, Köcher T, Pichler P, Novatchkova M, Yang J, Schlögelhofer P, Mechtler K. (2015) Quantitative phosphoproteomics of the ataxia telangiectasia-mutated (ATM) and ataxia telangiectasia-mutated and rad3-related (ATR) dependent DNA damage response in *Arabidopsis thaliana*. Molecular and Cellular Proteomics **14**, 556–571. https://doi.org/10.1074/mcp.M114.040352

Roychowdhury A, Kundu A, Bose M, Gujar A, Mukherjee S, Das AK. (2015) Complete catalytic cycle of cofactor-independent phosphoglycerate mutase involves a spring-loaded mechanism. The FEBS Journal **282**, 1097–1110. https://doi.org/10.1111/febs.13205

Sasaki Y, Kozaki A, Hatano M. (1997) Link between light and fatty acid synthesis: Thioredoxin-linked reductive activation of plastidic acetyl-CoA carboxylase. Proceedings of the National Academy of Sciences of the United States of America **94**, 11096–11101. https://doi.org/10.1073/pnas.94.20.11096

Scheible WR, Krapp A, Stitt M. (2000) Reciprocal diurnal changes of phosphoenolpyruvate carboxylase expression and cytosolic pyruvate kinase, citrate synthase and NADP-isocitrate dehydrogenase expression regulate organic acid metabolism during nitrate assimilation in tobacco leaves. Plant, Cell and Environment **23**, 1155–1167. https://doi.org/10.1046/j.1365-3040.2000.00634.x

Smith GC, Hass LF. (1985) Wheat germ phosphoglycerate mutase: Purification, polymorphism, and inhibition. Biochemical and Biophysical Research Communications **131**, 743–749. https://doi.org/10.1016/0006-291X(85)91301-4

Stein M, Gabdoulline RR, Wade RC. (2010) Cross-species analysis of the glycolytic pathway by comparison of molecular interaction fields. Molecular BioSystems **6**, 152–164. https://doi.org/10.1039/B912398A

Stitt M, ap Rees T. (1978) Pathways of carbohydrate oxidation in leaves of *Pisum sativum* and *Triticum aestivum*. Phytochemistry **17**, 1251–1256. https://doi.org/10.1016/S0031-9422(00)94566-7

Streatfield SJ, Weber A, Kinsman EA, Häusler RE, Li J, Post-Beittenmiller D, Kaiser WM, Pyke KA, Flügge UI, Chory J. (1999) The phospho*enol*pyruvate/phosphate translocator is required for phenolic metabolism, palisade cell development, and plastid-dependent nuclear gene expression. The Plant Cell **11**, 1609–1622. https://doi.org/10.1105/tpc.11.9.1609

Sun R, Qin S, Zhang T, Wang Z, Li H, Li Y, Nie Y. (2019) Comparative phosphoproteomic analysis of blast resistant and susceptible rice cultivars in response to salicylic acid. BMC Plant Biology **19**, 454. https://doi.org/10.1186/s12870-019-2075-5

Sweetlove LJ, Beard KFM, Nunes-Nesi A, Fernie AR, Ratcliffe RG. (2010) Not just a circle: Flux modes in the plant TCA cycle. Trends in Plant Science **15**, 462–470. https://doi.org/10.1016/j.tplants.2010.05.006

Tcherkez G, Bligny R, Gout E, Mahé A, Hodges M, Cornic G. (2008) Respiratory metabolism of illuminated leaves depends on CO_2 and O_2 conditions. Proceedings of the National Academy of Sciences of the United States of America **105**, 797–802. https://doi.org/10.1073/pnas.0708947105

Tcherkez G, Boex-Fontvieille E, Mahé A, Hodges M. (2012) Respiratory carbon fluxes in leaves. Current Opinion in Plant Biology **15**, 308–314. https://doi.org/10.1016/j.pbi.2011.12.003

Tcherkez G, Mahé A, Gauthier P, Mauve C, Gout E, Bligny R, Cornic G, Hodges M. (2009) *In folio* respiratory fluxomics revealed by ^{13}C isotopic labeling and H/D isotope effects highlight the noncyclic nature of the tricarboxylic acid 'cycle' in illuminated leaves. Plant Physiology **151**, 620–630. https://doi.org/10.1104/pp.109.142976

Tovar-Méndez A, Miernyk JA, Randall DD. (2003) Regulation of pyruvate dehydrogenase complex activity in plant cells. European Journal of Biochemistry **270**, 1043–1049. https://doi.org/10.1046/j.1432-1033.2003.03469.x

Umezawa T, Sugiyama N, Takahashi F, Anderson JC, Ishihama Y, Peck SC, Shinozaki K. (2013) Genetics and phosphoproteomics reveal a protein phosphorylation network in the abscisic acid signaling pathway in *Arabidopsis thaliana*. Science Signaling **6**, 6–8. https://doi.org/10.1126/scisignal.2003509

Urbanczyk-Wochniak E, Baxter C, Kolbe A, Kopka J, Sweetlove LJ, Fernie AR. (2005) Profiling of diurnal patterns of metabolite and transcript abundance in potato (*Solanum tuberosum*) leaves. Planta **221**, 891–903. https://doi.org/10.1007/s00425-005-1483-y

Voll LM, Hajirezaei MR, Czogalla-Peter C, Lein W, Stitt M, Sonnewald U, Börnke F. (2009) Antisense inhibition of enolase strongly limits the metabolism of aromatic amino acids, but has only minor effects on respiration in leaves of transgenic tobacco plants. New Phytologist **184**, 607–618. https://doi.org/10.1111/j.1469-8137.2009.02998.x

Wang X, Bian Y, Cheng K, Gu L-F, Ye M, Zou H, Sun SS-M, He J-X. (2013*a*) A large-scale protein phosphorylation analysis reveals novel phosphorylation motifs and phosphoregulatory networks in Arabidopsis. Journal of Proteomics **78**, 486–498. https://doi.org/10.1016/j.jprot.2012.10.018

Wang X, Bian Y, Cheng K, Zou H, Sun SS-M, He J-X. (2012) A Comprehensive differential proteomic study of nitrate deprivation in Arabidopsis reveals complex regulatory networks

of plant nitrogen responses. Journal of Proteome Research **11**, 2301–2315. https://doi.org/10.1021/pr2010764

Wang P, Xue L, Batelli G, Lee S, Hou Y-J, Van Oosten MJ, Zhang H, Tao WA, Zhu J-K. (2013*b*) Quantitative phosphoproteomics identifies SnRK2 protein kinase substrates and reveals the effectors of abscisic acid action. Proceedings of the National Academy of Sciences of the United States of America **110**, 11205–11210. https://doi.org/10.1073/pnas.1308974110

Westram A, Lloyd JR, Roessner U, Riesmeier JW, Kossmann J. (2002) Increases of 3‐phosphoglyceric acid in potato plants through antisense reduction of cytoplasmic phosphoglycerate mutase impairs photosynthesis and growth, but does not increase starch contents. Plant, Cell and Environment **25**, 1133–1143. https://doi.org/10.1046/j.1365-3040.2002.00893.x

Xing A, Last RL. (2017) A regulatory hierarchy of the Arabidopsis branched-chain amino acid metabolic network. Plant Cell **29**, 1480–1499. https://doi.org/10.1105/tpc.17.00186

Xue L, Wang P, Wang L, Renzi E, Radivojac P, Tang H, Arnold R, Zhu J-K, Tao WA. (2013) Quantitative measurement of phosphoproteome response to osmotic stress in Arabidopsis based on library-assisted extracted ion chromatogram (LAXIC). Molecular and Cellular Proteomics **12**, 2354–2369. https://doi.org/10.1074/mcp.O113.027284

Yamada K, Lim J, Dale JM, *et al.* (2003) Empirical analysis of transcriptional activity in the Arabidopsis genome. Science **302**, 842–846. https://doi.org/10.1126/science.1088305

Yang Z, Guo G, Zhang M, Liu CY, Hu Q, Lam H, Cheng H, Xue Y, Li J, Li N. (2013) Stable isotope metabolic labeling-based quantitative phosphoproteomic analysis of Arabidopsis mutants reveals ethylene-regulated time-dependent phosphoproteins and putative substrates of constitutive triple response 1 kinase. Molecular and Cellular Proteomics **12**, 3559–3582. https://doi.org/10.1074/mcp.M113.031633

Yu H, Dranchak P, Li Z, MacArthur R, Munson M S, Mehzabeen N, Baird N J, Battalie K P, Ross D, Lovell S, Carlow C K S, Suga H, Inglese J (2017) Macrocycle peptides delineate locked-open inhibition mechanism for microorganism phosphoglycerate mutases. Nature Communications **8**, 14932. https://doi.org/10.1038/ncomms14932

Zhang Y, Foster JM, Kumar S, Fougere M, Carlow CKS. (2004) Cofactor-independent phosphoglycerate mutase has an essential role in *Caenorhabditis elegans* and is conserved in parasitic nematodes. Journal of Biological Chemistry **279**, 37185–37190. https://doi.org/10.1074/jbc.M405877200

Zhang H, Zhou H, Berke L, Heck AJR, Mohammed S, Scheres B, Menke FLH. (2013) Quantitative phosphoproteomics after auxin-stimulated lateral root induction identifies an SNX1 protein phosphorylation site required for growth. Molecular and Cellular Proteomics **12**, 1158–1169. https://doi.org/10.1074/mcp.M112.021220

Zhao Z, Assmann SM. (2011) The glycolytic enzyme, phosphoglycerate mutase, has critical roles in stomatal movement, vegetative growth, and pollen production in *Arabidopsis thaliana*. Journal of Experimental Botany **62**, 5179–5189. https://doi.org/10.1093/jxb/err223

Table legends

Table 1: Metabolite levels of organic acids, fatty acids, shikimate and associated aromatic amino acids, and branched-chain amino acids from light- and light/dark-treated Arabidopsis rosette leaves

Values are mean ± SD metabolite levels (arbitrary units per g DW) from n=3 independent biological replicates of light- and light/dark-treated Arabidopsis plants. Asterisks correspond to significant difference values between the 2 treatments with the following p-values: **⩽ 0.01, *⩽0.05 (2-tailed Student's *t*-test).

Figure Legends

Figure 1: **Phosphorylation status of *At*iPGAM1/2 phosphopeptide in light- and light/dark-treated Arabidopsis**

The histogram shows *At*iPGAM1/2 phosphopeptide amounts in rosette leaves from plants initially grown under a short day (8/16 h light/dark) then given either a 4 h light (light) treatment or the same 4 h light followed by a 2 h dark (light/dark) treatment during the natural 8 h day period and further analyzed as previously described by Boex-Fontvieille *et al.*, (2014). Phosphoproteomics analyses were carried with three biological replicates. Statistical significance was determined by a Student's *t*-test (*p<0.01).

Figure 2: *At*iPGAM2 3D-structure model

Using both modelling and the repository tools of SWISS-MODEL, the 3D structure of *At*iPGAM2 was predicted. (**a**) The protein sequence alignment of *At*iPGAM2 (Model_01) and *Leshmania mexicana* iPGAM (3igy.1.A) (see Figure S2 for its 3D-structure). The two protein sequences share 56.3 % sequence identity. Purple boxes indicate α-helices and green arrows β-sheets. (**b**) The rainbow-colored 3D-structure of *At*iPGAM2 (A0A384KAQ5 from the SWISS-MODEL Repository database) built using 3igy.1 as template with a global model quality estimation (GMQE) of 0.8 (on a scale from 0 to 1). The phosphatase and transferase domains (A and B, respectively) are indicated. This structure includes two metal ions (pink balls) and 3-PGA (see Figure S2 for a Qualitative Model Energy ANalysis (QMEAN) representation). (**c**) The catalytic core of the enzyme. Insert shows the position of the

focused region. Note that the presented view corresponds to a 180° turn compared to that given in (**b**). The catalytic serine is marked in green on the chain (S82). All residues involved in metal ion and 3-PGA binding are licorice represented and the two Co^{2+} ions (Co1 and Co2) are included (pink balls). The two residues studied in this work are annotated in black (D29 and R290) and their closest neighbors in dark grey (D472, H473, H141 and R207; for others see Figure S3). Purple lines represent the five interactions of each metal ion with both 3-PGA and the chain. Blue and yellow lines represent respectively the three H-bonds and the 14 salt bridges of the 3-PGA with the chain. Each bond is separately detailed in Figure S3.

Figure 3: 3-PGA-dependent S82 phosphorylation of recombinant *At*iPGAM2

The effects of 3-PGA concentration and Mg^{2+}-dependence on *in vitro At*iPGAM2 phosphorylation were analysed. Recombinant *At*iPGAM2$_{WT}$ was incubated for 10 min either in the presence of different 3-PGA concentrations or in the absence of 5 mM Mg^{2+} (with 2.5 mM 3-PGA), separated on SDS-PAGE gels before *At*iPGAM phosphopeptide amounts were estimated using LC-MS/MS peak areas of phospho-S82 (OP) and non-phosphorylated S82 (OH) containing peptides. The OP/OH ratios were then normalized to those obtained for *At*iPGAM2 in the presence of 5 mM 3-PGA. Values are means ± SD (n=4 biological replicates) and statistical significance determined by a Student's *t*-test (*$p<0.01$) is shown with respect to 0 mM 3-PGA.

Figure 4: S82 phosphorylation of recombinant *At*iPGAM2 with altered catalytic mechanism properties

The effect of active site-specific mutations that alter either 3-PGA binding (R290L) or phosphate transferase activity (D29N) on the amounts of detected *At*iPGAM2 phosphopeptide. Recombinant *At*iPGAM2$_{WT}$, *At*iPGAM2$_{D29N}$ and *At*iPGAM2$_{R290L}$ were incubated with/without 3-PGA (0 mM and 2.5 mM), and separated on SDS-PAGE gels before *At*iPGAM phosphopeptide amounts were estimated using LC-MS/MS peak areas of phospho-S82 (OP) and non-phosphorylated S82 (OH) containing peptides. Value are means ± SD (n=3 biological replicates) and statistical significance was determined by a Student's *t*-test (*$p<0.05$).

Figure 5: A simplified scheme of PEP and pyruvate-related metabolic pathways and significant changes in metabolite levels observed between light- and light/dark-treated Arabidopsis rosette leaves

In the light, photosynthetic CO_2 assimilation by Rubisco leads to the production of 3-PGA which is converted to triose phosphates *via* the Calvin cycle. Triose-phosphates can be used to make RuBP and starch or exported to the cytosol *via* a triose-phosphate transporter to make sugars and precursors (PEP and pyruvate) for several metabolic pathways including the TCA cycle in mitochondria, and saturated fatty acid, isoprenoids, branched-chain and aromatic amino acids in chloroplasts. Based on the amount of S82-phosphopeptide, iPGAM activity was higher in our light-treated compared to light/dark-treated Arabidopsis rosettes. Metabolite profiling showed that in our experimental conditions, saturated fatty acids accumulated in the light while organic acids associated with the TCA cycle increased in the dark. Shikimate and aromatic amino acid levels appeared to be insensitive to the treatments while amongst the three branched-chain amino acids only isoleucine (Ile) levels were significantly increased by the additional dark treatment. Colour codes: Metabolites found to be higher in the light (green), lower in the light (red), no significant difference (blue), not measured (black); ** and * indicate significantly different metabolite levels between the light and light/dark treatments with p-values of $\leqslant 0.01$ and $\leqslant 0.05$, respectively (2-tailed Student's *t*-test). Enzymes (boxed)/pathways activated in the light (green), inactivated in the light (red), unchanged in the light (blue). In the light, the TCA cycle operates in both reverse and forward directions (green lines) (see Tcherkez *et al.*, 2009). Abbreviations: RuBP, ribulose-1,5-bisphosphate; 3-PGA, 3-phosphoglycerate; 2-PGA, 2-phosphoglycerate; PEP, phospho*enol*pyruvate; OAA, oxaloacetate; 2-OG, 2-oxoglutarate; Rubisco, RuBP carboxylase/oxygenase; ACCase, acetyl-CoA carboxylase; PEPc, PEP carboxylase; PDH, pyruvate dehydrogenase; MEP, 2-*C*-methyl-d-erythritol 4-phosphate.

Table 1: Metabolite levels of organic acids, fatty acids, shikimate and associated aromatic amino acids, and branched-chain amino acids from light- and light/dark-treated Arabidopsis rosette leaves

	Light	Light/Dark	Light to Light/Dark ratio
Organic acids			
Pyruvic acid	0.76 ± 0.13	0.96 ± 0.05	0.80
Citric acid**	0.45 ± 0.14	0.99 ± 0.08	0.45
Succinic acid**	0.51 ± 0.14	1.84 ± 0.26	0.28
Fumaric acid	75.57 ± 48.46	150.31 ± 28.81	0.50
Malic acid*	2.03 ± 0.33	2.85 ± 0.01	0.71
Fatty acids			
Octanoic acid, C8:0	0.17 ± 0.03	0.16 ± 0.00	1.07
Lauric acid, C12:0*	1.03 ± 0.22	0.20 ± 0.01	5.05
Tetradecanoic acid, C14:0	0.54 ± 0.01	0.58 ± 0.02	0.92
Palmitic acid, C16:0*	9.09 ± 1.38	4.41 ± 0.21	2.06
Stearic acid, C18:0*	16.68 ± 3.13	3.96 ± 0.42	4.22
Linolenic acid, C18:3	0.07 ± 0.01	0.06 ± 0.03	1.01
Shikimate pathway			
Shikimic acid	1.03 ± 0.22	1.28 ± 0.12	0.80
Phenylalanine	0.36 ± 0.07	0.27 ± 0.07	1.34
Tyrosine	0.12 ± 0.01	0.13 ± 0.01	0.89
Branched-chain amino acids			
Isoleucine**	0.92 ± 0.11	1.39 ± 0.02	0.67
Leucine	0.43 ± 0.14	0.36 ± 0.09	1.19
Valine	3.68 ± 0.57	4.31 ± 0.39	0.85

Values are mean ± SD metabolite levels (arbitrary units per g DW) from n=3 independent biological replicates of light- and light/dark-treated Arabidopsis plants. Asterisks correspond to significant difference values between the 2 treatments with the following p-values: **$\leqslant$ 0.01, *$\leqslant$0.05 (2-tailed Student's *t*-test).

Figure 1

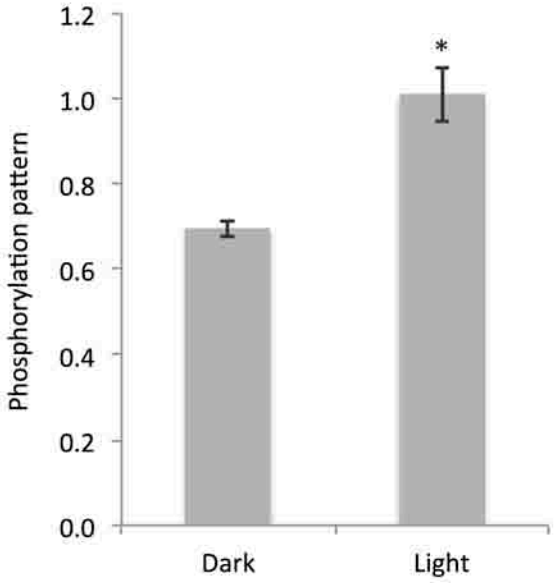

Figure 2

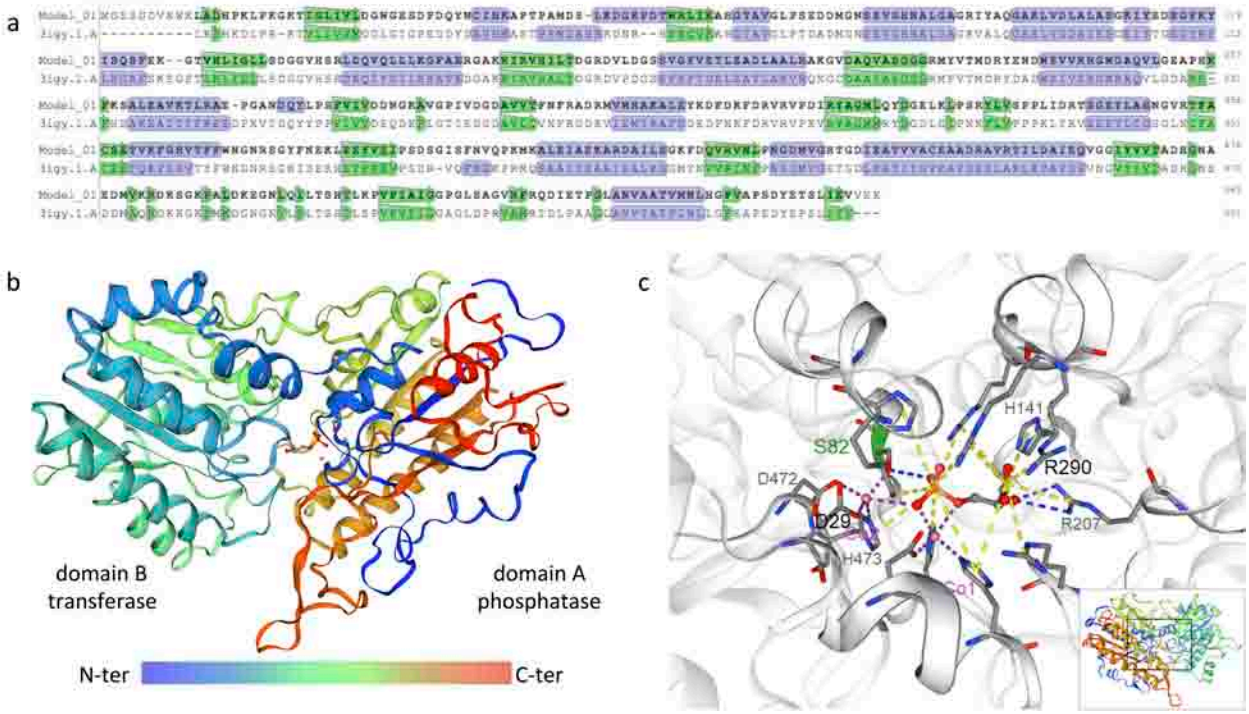
a
b
domain B
transferase
domain A
phosphatase
N-ter
C-ter
c
S82
H141
R290
D472
D29
R207
H473
Ca1

Figure 3

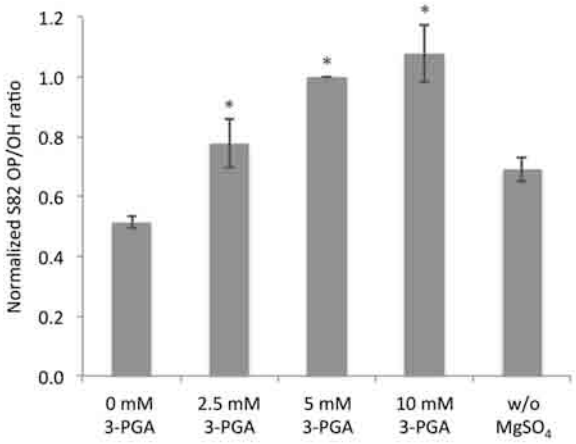
Normalized S82 OP/OH ratio
1.2
1.0
0.8
0.6
0.4
0.2
0.0
*
*
*
0 mM 3-PGA
2.5 mM 3-PGA
5 mM 3-PGA
10 mM 3-PGA
w/o $MgSO_4$

Figure 4

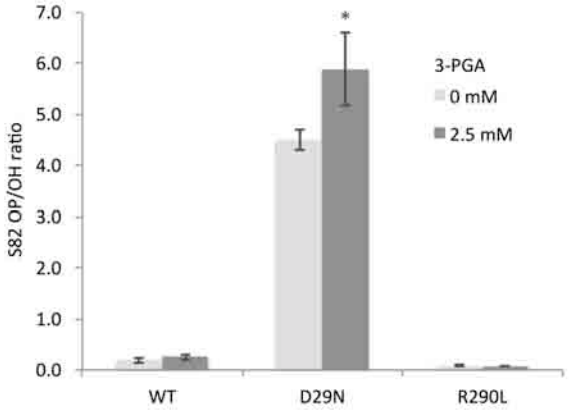
7.0
6.0
5.0
4.0
3.0
2.0
1.0
0.0
S82 OP/OH ratio
*
3-PGA
0 mM
2.5 mM
WT
D29N
R290L

Figure 5

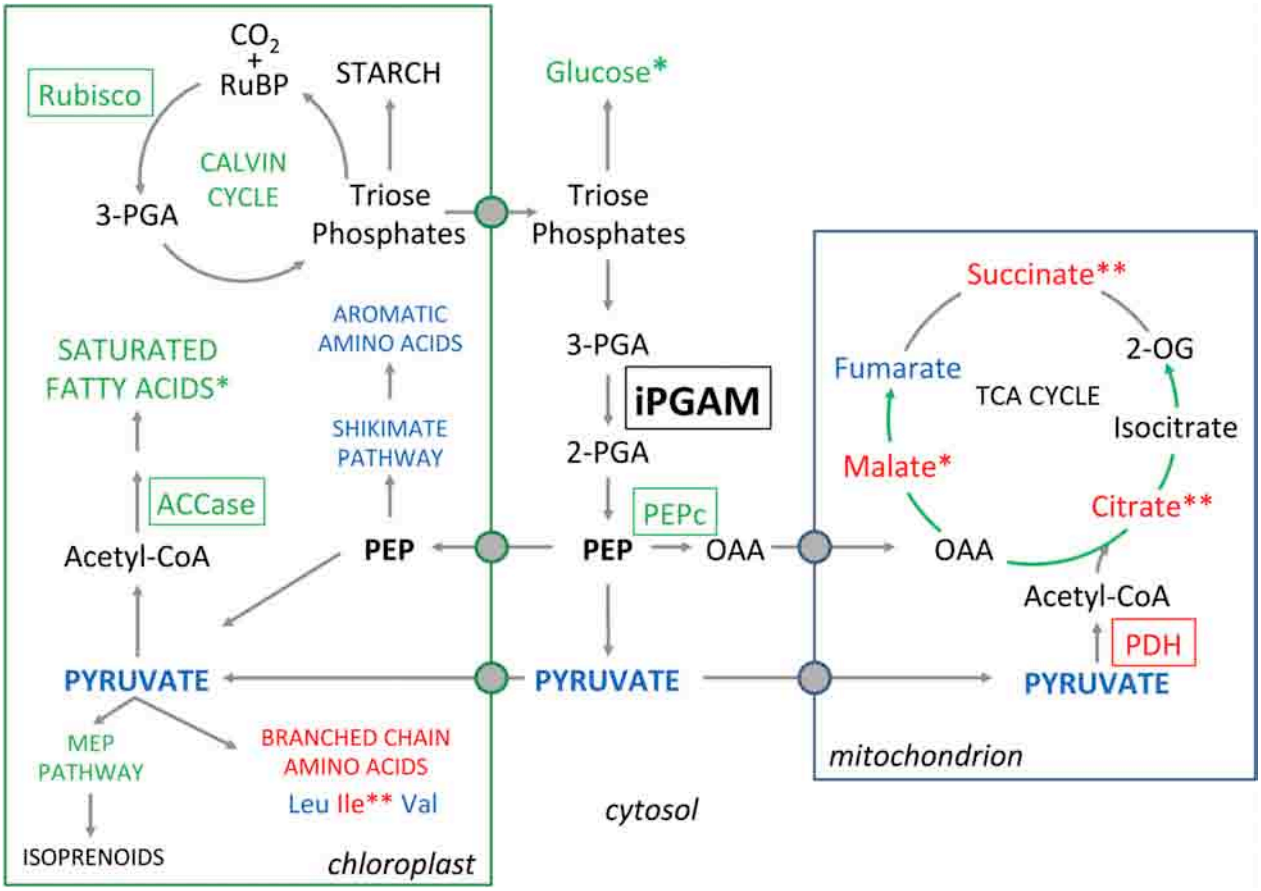
CO_2
+
RuBP
Rubisco
STARCH
CALVIN
CYCLE
3-PGA
Triose
Phosphates
Glucose*
Triose
Phosphates
3-PGA
iPGAM
2-PGA
PEPc
AROMATIC
AMINO ACIDS
SATURATED
FATTY ACIDS*
SHIKIMATE
PATHWAY
ACCase
Acetyl-CoA
PEP
PEP
OAA
PYRUVATE
PYRUVATE
MEP
PATHWAY
BRANCHED CHAIN
AMINO ACIDS
Leu Ile** Val
ISOPRENOIDS
chloroplast
cytosol
Succinate**
Fumarate
2-OG
TCA CYCLE
Isocitrate
Malate*
Citrate**
OAA
Acetyl-CoA
PDH
PYRUVATE
mitochondrion

Figure S1: Duminil et al.

```
                                   29                                                                82
AtiPGAM2   MGSSGDVNWKLADHPKLPKGKTIGLIVLDGWGESDPDQYNCIHKAPTPAMDSLKDGKPDTWRLIKAHGTAVGLPSEDDMGNSEVGHNALG 90
T.brucei   ------MALTLAAHKTLPRRK-LVLVVLDGVGIGPRDEYDAVHVAKTPLMDALFN-DPKHFRSICAHGTAVGLPTDADMGNSEVGHNALG 82
L.mexica   -----MSNLLLKLHKDLPRRK-LLIVVMDGLGIGPEDDYDAVHMASTPFMDAQRQ-NSRHFRSVRAHGTAVGLPTDADMGNSEVGHNALG 83
S.aureus   -----------------MAKKPTALIILDGFANRESEHGNAVKLANKPNFDRYYNKYPT--TQIEASGLDVGLPE-GQMGNSEVGHMNIG 70
B.anthra   -----------------MRKPTALIILDGFGLREETYGNAVAQAKKPNFDGYWNKFPH--TTLTACGEAVGLPE-GQMGNSEVGHLNIG 69
G.stearo   -----------------MSKKPVALIILDGFALRDETYGNAIAQANKPNFDRYWNEYPH--TTLKACGEAVGLPE-GQMGNSEVGHLNIG 70
                                *   ::::** .       :.:  * .* :*   :        : * *  ****   :********  :*

                                                                141                           171
AtiPGAM2   AGRIYAQGAKLVDLALASGKIYEDEGFKYISQSFE--KGTVHLIGLLSDGGVHSRLDQVQLLLKGFAERGAKRIRVHILTDGRDVLDGSS 178
T.brucei   AGRVVLQGASLVDDALESGEIFTSEGYRYLHGAFSQPGRTLHLIGLLSDGGVHSRDNQVYQILKHAGANGAKRIRVHALYDGRDVPDKTS 172
L.mexica   AGRVVLQGASLVDDALKSGEIFTGEGYRYLLGACSKEDSTLHLIGLLSDGGVHSRDNQIYSIIERAAKDGAKRIRVHVLYDGRDVPDGSS 173
S.aureus   AGRIVYQSLTRINKSIEDGDFFENHVLNNAIAHVNSHDSALHIFGLLSDGGVHSHYKHLFALLELAKKQGVEKVYVHAFLDGRDVDQKSA 160
B.anthra   AGRIVYQSLTRVNVAIREGEFDKNETFQSAIKSVKEKGTALHLFGLLSDGGVHSHMNHMFALLRLAAKEGVEKVYIHAFLDGRDVGPKTA 159
G.stearo   AGRIVYQSLTRVNIAIREGEFERNETFLAAMNHVKQHGTSLHLFGLLSDGGVHSHIHHLYALLRLAAKEGVKRVYIHGFLDGRDVGPQTA 160
           ***:  *. . :: :: .*.:  ..         .    ::*::**********: .::  ::.     *.::: :* : *****   ::

                                   207    214
AtiPGAM2   VGFVETLEADLAALRAKGVDAQVASGGGRMYVTMDRYENDWSVVKRGWDAQVLGEAPHKFKSALEAVKTLR-AEPGANDQYLPSFVIVDD 267
T.brucei   FKFTDELEEVLAKLREGGCDARIASGGGRMFVTMDRYEADWSIVERGWRAQVLGEGRA-FKSAREALTKFREEDANISDQYYPPFVIAGD 261
L.mexica   FRFTEELEAVLAKVRQDGCDAAIASGGGRMFVTMDRYEADWSIVERGWKAQVLGDARH-FRSAKEAITTFREEDPKVTDQYYPPFVVVDE 262
S.aureus   LKYIEETEAKFNELGIG----QFASVSGRYY-AMDR-DKRWEREEKAYNAIRNFDAPT-YATAKEGVEAS--YNEGLTDEFVVPFIVENQ 241
B.anthra   QSYIDATNEVIKETGVG----QFATISGRYY-SMDR-DKRWDRVEKCYRAMVNGEGPT-YKSAEECVEDS--YANGIYDEFVLPSVIVNE 240
G.stearo   PQYIKELQEKIKEYGVG----EIATLSGRYY-SMDR-DKRWDRVEKAYRAMVYGEGPT-YRDPLECIEDS--YKHGIYDEFVLPSVIVRE 241
             : .  :  :          .*: .** : :*** :  *.  :: : *    :.   :    * :          *::    ::  :

                              287  290
AtiPGAM2   NGKAVGPIVDGDAVVTFNFRADRMVMHAKALEYKDFDKFDRVR--VPDIRYAGMLQYDGELKLPSRYLVSPPLIDRTSGEYLAHNGVRTF 355
T.brucei   DGRPIGTIEDGDAVLCFNFRGDRVIEMSRAFEEEEFDKFNRVR--LPKVRYAGMMRYDGDLGIPNNFLVPPPKLTRTSEEYLIGSGCNIF 349
L.mexica   QDKPLGTIEDGDAVLCVNFRGDRVIEMTRAFEDEDFAKFDRVR--VPKVRYAGMMRYDGDLGIPNNFLVPPPKLTRVSEEYLCGSGLKIF 350
S.aureus   N----DGVNDGDAVIFYNFRPDRAAQLSEIFANRAFEGFKVEQ--VKDLFYATFTKYNDNID--AVIVFEKVDLNNTIGEIAQNNNLTQL 323
B.anthra   DNTPVATINDDDAVIFYNFRPDRAIQIARVFTNGDFREFDRGEKVPHIPEFVCMTHFSETVD--GYVAFKPMNLDNTLGEVVAQAGLKQL 328
G.stearo   DGRPVATIQDNDAIIFYNFRPDRAIQISNTFTNEDFREFDRGPKHPKHLFFVCLTHFSETVK--GYVAFKPTNLDNTIGEVLSQHGLRQL 329
           :      : *.**::  *** **    :. :    *  *.          :. : ::.  :       .    : ..  *     .   :

              362  365                                                                431  435
AtiPGAM2   ACSETVKFGHVTFFWNGNRSGYFNEKLEEYVEIPSDSGISFNVQPKMKALEIAEKARDAILSGKFDQVRVNLPNGDMVGHTGDIEATVVA 445
T.brucei   ALSETQKFGHVTYFWNGNRSGKLSEERETFCEIPSDR-VQFNQKPLMKSKEITDAAVDAIKSGKYDMIRINYPNGDMVGHTGDLKATITS 438
L.mexica   ACSETQKFGHVTYFWNGNRSGKIDDEHETFKEVPSDR-VHFNKQPKMKSAEITEAAIEALKGGMYDVVRINFPNGDMVGHTGDLKATIVG 439
S.aureus   RIAETEKYPHVTYFMSGGRNEEFIGERRRLIDSP--KVATYDLKPEMSAYEVKDALLEELNKGDLDLIILNFANPDMVGHSGMLEPTIKA 411
B.anthra   RIAETEKYPHVTFFFSGGREAEFPGEERILINSP--KVATYDLKPEMSIYEVTDALVNEIENDKHDVIILNFANCDMVGHSGMMEPTIKA 416
G.stearo   RIAETEKYPHVTFFMSGGREEKFPGEDRILINSP--KVPTYDLKPEMSAYEVTDALLKEIEADKYDAIILNYANPDMVGHSGKLEPTIKA 417
             :** *: ***:* .*.*.  :  : .   : *      :: :* *.  *: :   . :  .  * : :*  * *****:* :: *: .

                                  472473                          502
AtiPGAM2   CEAADRAVRTILDAIEQVGGIYVVTADHGNAEDMVKRDKSGKPALDKEGNLQILTSHTLKPVPIAIGGPGLSAGVRFRQDIETPGLANVA 535
T.brucei   LEAVDQSLQRLKEAVDSVNGVFLITADHGNSDDMVQRDKKGKPVRDAEGNLMPLTSHTLAPVPVFIGGAGLDPRVQMRTDLPRAGLANVT 528
L.mexica   VQAVDESLAKLKDAVDNVNGVFIVTADHGNSDDMAQRDKKGKPIKDEKGNVLPLTSHTLSPVPVFIGGAGLDPRVKMRTDMPAAGLANVT 529
S.aureus   IEAVDECLGEVVDKILDMDGYAIVTADHGNSDQVLTDDD------------QPMTTHTTNPVPVIVTKEGVTLRE-------TGRLGDLA 482
B.anthra   VEATDECLGKVVEAILAKDGVALITADHGNADEELTSEG------------EPMTAHTTNPVPFIVTKNDVELRE-------DGILGDIA 487
G.stearo   VEAVDECLGKVVDAILAKGGIAIITADHGNADEVLTPDG------------KPQTAHTTNPVPVIVTKKGIKLRD-------GGILGDLA 488
            :*.*..:  : : :   .*  ::******:::    :                *:**  ***. :   .:              *.:::

AtiPGAM2   ATVMNLHGFVAPSDYETSLIEVVEK 560
T.brucei   ATFINLMGFEAPSDYEPSLIEVA-- 551
L.mexica   ATFINLLGFEAPEDYEPSLICVEN- 553
S.aureus   PTLLDLLNVEQPEDMTGESLIKH-- 505
B.anthra   PTMLTLLGVEQPKEMTGKTIIK--- 509
G.stearo   PTMLDLLGLPQPNEMTGKSLIVK-- 511
            *.: * ..  *.:   . :
```

Figure S2: Duminil et al.

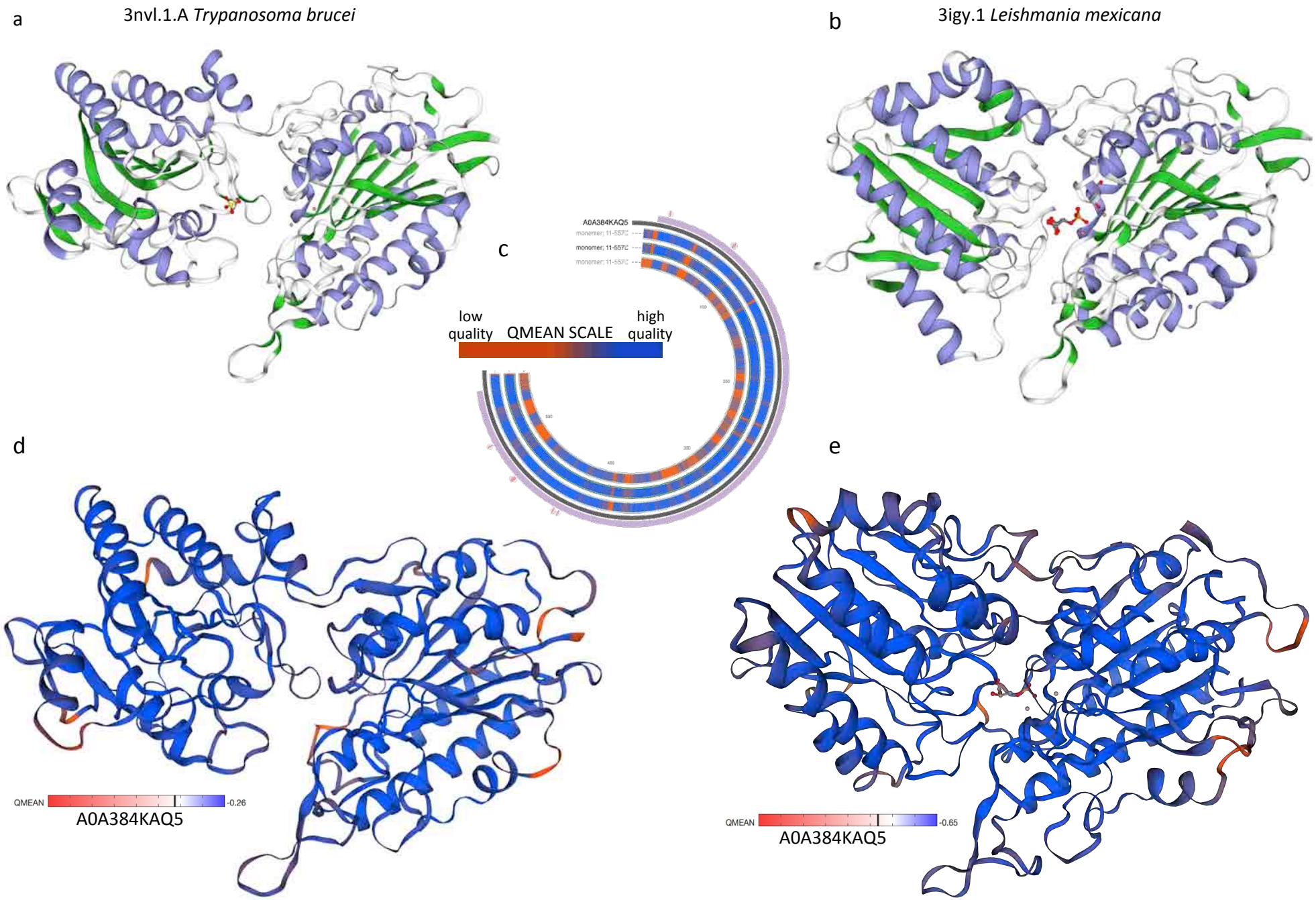

Figure S3: Duminil et al.

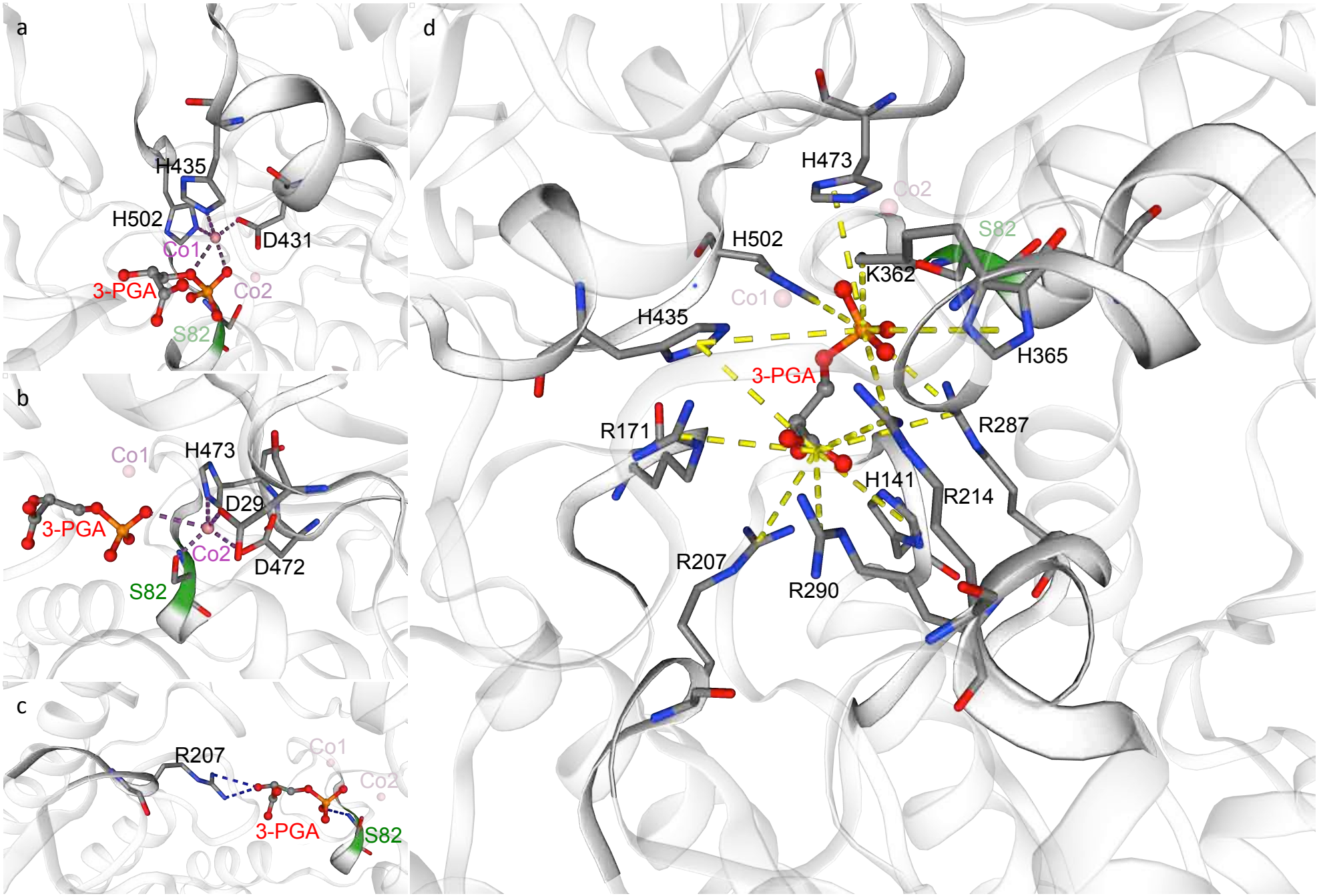

Figure S4: Duminil et al.

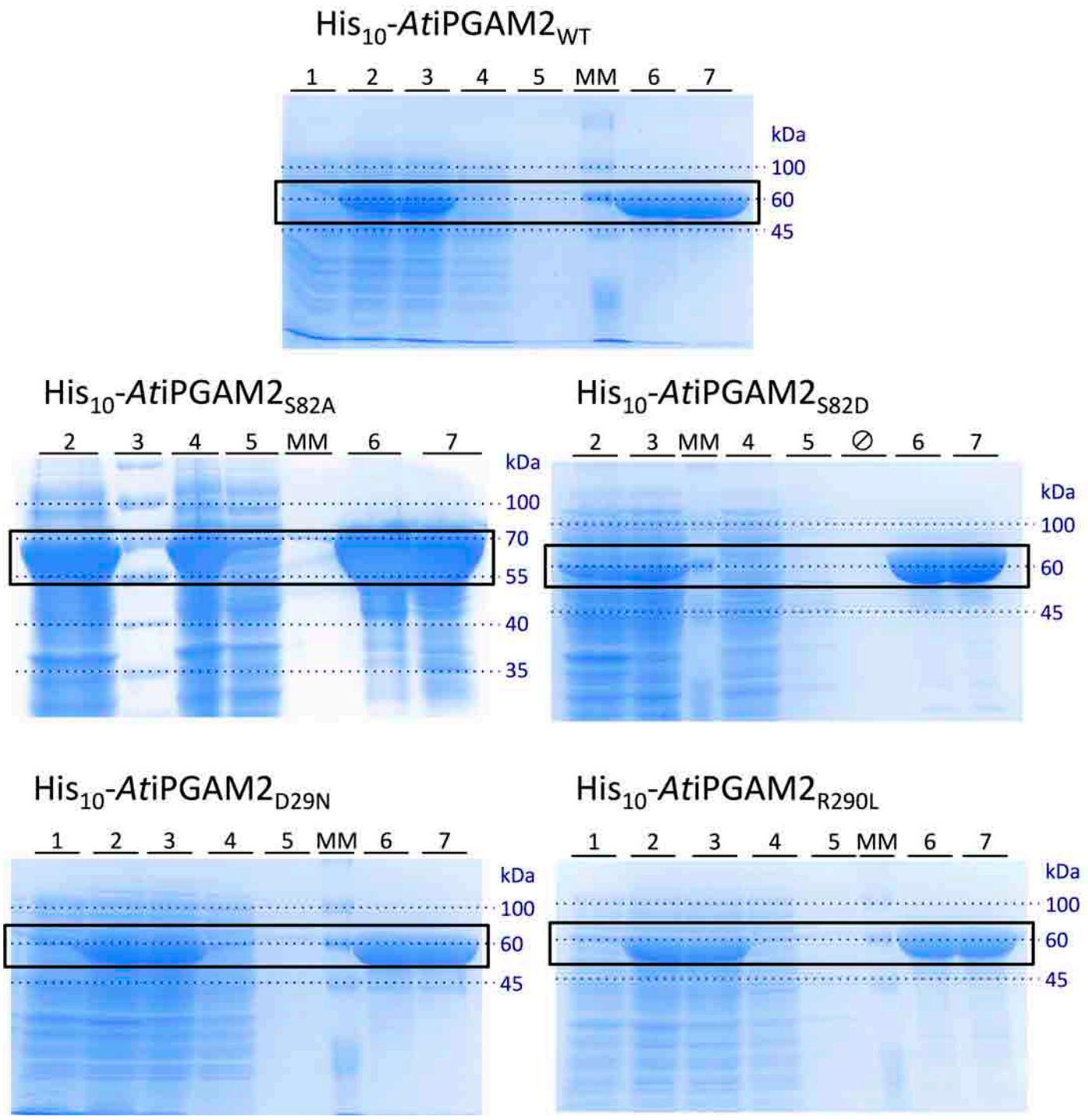

Figure S5: Duminil et al.

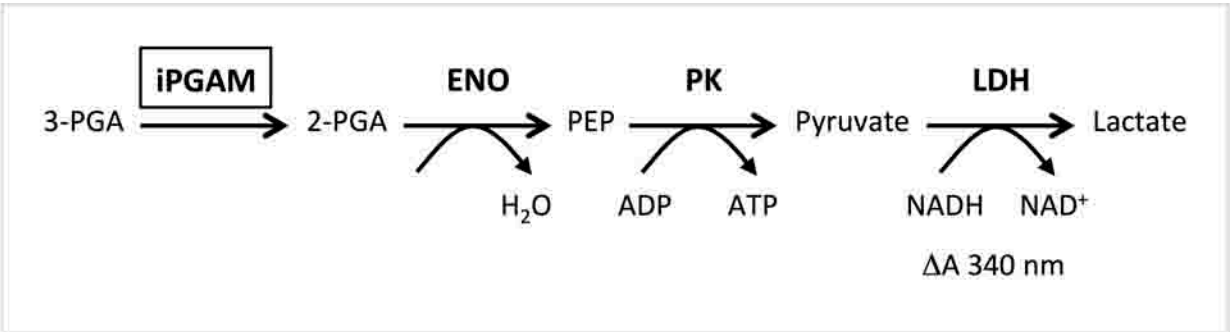

Figure S6: Duminil et al.

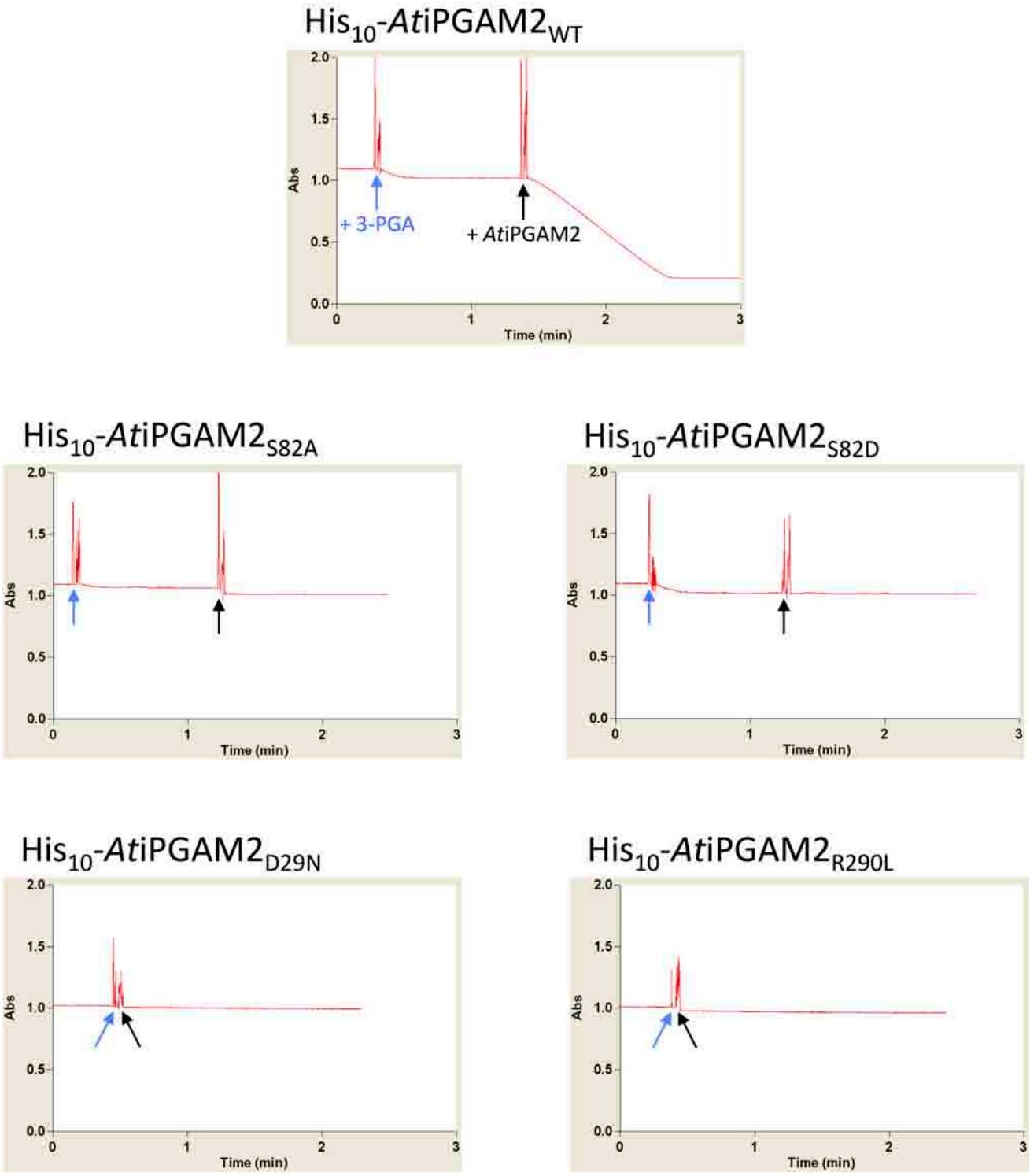

Supporting information

Supporting figure legends

Figure S1: Protein sequence alignments between *At*iPGAM2 and non-plant iPGAMs with resolved 3D-structures.

A multiple sequence alignment of iPGAM proteins was performed using Clustal Omega (1.2.4) with the following sequences indicated by their National Center for Biotechnology Information accession number: *Arabidopsis thaliana* BAH19613 (AtiPGAM2), *Trypanosoma brucei* EAN78199 (T.brucei) and *Leishmania mexicana* XP_003875025 (L.mexica) for family 1 enzymes and *Staphylococcus aureus* AGU54589 (S.aureus), *Bacillus anthracis* OON48717 (B.anthra) and *Geobacillus stearothermophilus* KYD33754 (G.stearo) for enzymes belonging to family 2. All residues involved in the catalytic core (see also Figure S3) are shown in bold (numbering of the *At*iPGAM2 sequence), in green the catalytic serine (S82), in blue the two residues (D29 and R290) studied in this work and in dark-red all of the others (H141, R171, R207, R214, R287, K362, H365, D431, H435, D472, H473 and H502). (*) are identical residues and (: or .) are strongly or poorly similar residues. Purple and blue-green shadowings indicate residues involved in the phosphatase and the transferase domains respectively according to coordinates described for *T. brucei* (Mercaldi *et al.*, 2012) and for *B. anthracis* (Nukui *et al.*, 2007) enzymes.

Figure S2: 3D structure of templates used for *At*iPGAM2 structure prediction.

Predicted *At*iPGAM2 3D structures and their corresponding iPGAM templates are taken from the SWISS-MODEL Repository entry A0A384KAQ5_ARATH_iPGAM2. (**a, b**) 3D-structures of the two templates used to predict *At*iPGAM2 structure with α-helices in purple and β-sheets in green. (**a**) 3nvl.1.A corresponds to the crystal structure of *Trypanosoma brucei* iPGAM in the open conformation and containing one sulphate and two cobalt ions as ligands (Mercaldi *et al.*, 2012). (**b**) 3igy.1 corresponds to the crystal structure of *Leishmania mexicana* iPGAM in the closed conformation and containing two cobalt ions and 3-PGA as ligands (Nowicki *et al.*, 2009). (**c**) An estimation of the modelling quality along the *At*iPGAM2 sequence (A0A384KAQ5) with three different templates is shown using the QMEAN scale (from low quality (red) to high quality (blue)); from outside to the inside of the circle: with

3nvl.1.A, 3igy.1 and 5kgl.1 as templates. 5kgl.1 corresponds to the open structure of *Caenorhabditis elegans* iPGAM (Yu *et al.*, 2017) and it was discarded since it displayed a low QMEAN score -3.34. (**d**) The QMEAN scaled predicted structure of *At*iPGAM2 using 3nvl.1.A as template with 58.56 % sequence identity and a QMEAN score of -0.26. (**e**) The QMEAN scaled predicted structures of *At*iPGAM2 using 3igy.1 as template with 56.83 % sequence identity and a QMEAN score of -0.65.

Figure S3: *At*iPGAM2 structure prediction: catalytic core details.

(**a**-**d**) are details of the catalytic core in the *At*iPGAM2 predicted structure based on 3igy.1 that includes two Co^{2+} ions (Co1 and Co2, pink balls) and 3-PGA (C, O, P atoms are grey, red and orange balls, respectively). The catalytic serine 82 (S82) is coloured in green on the chain. All residues involved in the different bonds are licorice represented. (**a**) Depicts the interactions (purple broken lines) of the first Co^{2+} ion (Co1); three interactions with residues D431, H435 and H502 and two with 3-PGA. (**b**) Depicts the interactions (purple broken lines) of the second Co^{2+} ion (Co2); four interactions with residues D29, S82, D472 and H473 and one with 3-PGA. (**c**) Displays H-bonds (blue broken lines) between the 3-PGA and the chain, one bond with S82 and two with R207. (**d**) Shows the 14 salt bridges (yellow broken lines) between 3-PGA and the following residues: H141, R171, R207, R214 (2 bonds), R287 (2 bonds), R290, K362, H365, H435 (2 bonds), H473 and H502.

Figure S4: **Purification of *At*iPGAM2$_{WT}$, *At*iPGAM2$_{S82A}$, *At*iPGAM2$_{S82D}$, *At*iPGAM2$_{D29N}$ and *At*iPGAM2$_{R290L}$.**

SDS-PAGE gels were performed with protein samples collected at different purification steps of *At*iPGAM2$_{WT}$ (His$_{10}$-*At*iPGAM2$_{WT}$), *At*iPGAM2$_{S82A}$ (His$_{10}$-*At*iPGAM2$_{S82A}$), *At*iPGAM2$_{S82D}$ (His$_{10}$-*At*iPGAM2$_{S82D}$), *At*iPGAM2$_{D29N}$ (His$_{10}$-*At*iPGAM2$_{D29N}$) and *At*iPGAM2$_{R290L}$ (His$_{10}$-*At*iPGAM2$_{R290L}$), and stained with Coomassie blue. Numbers indicate the following purification steps: (**1**) Proteins from the total bacterial lysate before induction using IPTG; (**2**) Total proteins from IPTG-induced bacteria collected after the French press; (**3**) Soluble proteins harvested after centrifugation; (**4**) Pass-through proteins that did not fix to the Ni^{2+}-affinity resin; (**5**) Proteins collected after the first washing step; (**6**) Proteins eluted from the affinity resin using 250 mM imidazole; (**7**) Desalted proteins. (**MM**) corresponds to molecular weight markers.

Figure S5: ***At*iPGAM2 activity measurement with a coupled reaction.**

The diagram represents the coupled reaction used to measure the *At*iPGAM activity according to Zhang *et al.*, (2004): 3-PGA: 3-phosphoglycerate; 2-PGA: 2-phosphoglycerate; PEP: phospho*enol*pyrvuvate; iPGAM: cofactor independent-phosphoglycerate mutase; ENO: enolase; PK: pyruvate kinase; LDH: lactate dehydrogenase. Since every step is equimolar, recombinant *At*iPGAM2 activity can be measured by the disappearance of NADH detected with a spectrophotometer at $A_{340\ nm}$.

Figure S6: **3-PGA-dependent iPGAM activity of recombinant wild-type and mutated *At*iPGAM2 proteins**

Real-time Varian Cary 50 spectrophotometer traces measuring NADH oxidation at A_{340nm} and showing the requirement of specific residues for *in vitro At*iPGAM2 activity, as measured *via* the coupled reaction described in the Experimental Procedures and Figure S5. All iPGAM activities were measured after the addition of 1 mM 3-PGA (blue arrow) and 2.5 µg of recombinant protein (*At*iPGAM2$_{WT}$, *At*iPGAM2$_{S82A}$, *At*iPGAM2$_{S82D}$, *At*iPGAM2$_{D29N}$, *At*iPGAM2$_{R290L}$; black arrow). When S82, D29 or R290 was mutated, 3PGA-dependant iPGAM activity was abolished.

Supplementary Table S1: List of papers indexed in PhosPhAt 4.0 (http://phosphat.uni-hohenheim.de/), describing phosphoproteomic experiments in which S80/S82 of *Ati*PGAM1/2 was found phosphory

For each occurence of S82-containing phosphopeptide (AHGTAVGLPSEDDMGN(pS)EVGHNALGAGR), PubMed[uid], informations on the aim of the study, the plant material and growth conditions as well as details on light conditions are documente reference of thecorresponding paper. The last line in yellow describes the paper in which S75 was also annotated as phosphorylated, even if the peptide identified is the same. MS medium: Murashige and Skoog medium; MES: 2-(N-morpholino)et

PubMed[uid]	Aim of the study	Arabidopsis plant material and growth conditions	Light conditions
17934214	To gain proteomics insight into Arabidopsis cytosolic ribosomal composition and its post-translational modifications.	*Arabidopsis thaliana* cell culture	unspecified
19688752	To investigate protein phosphorylation in purified mitochondria from cell suspensions of the model plant *Arabidopsis thaliana*	An *Arabidopsis thaliana* (ecotype Lansberg erecta) cell culture established from callus of stem explants weekly subcultured in MS medium at 22 °C. Prior to mitochondrial isolations cell cultures are maintained in the dark for 7 days at 22 °C	continuous dark for 7 days prior mitochondrial isolation
20466843	To investigate the conservation of phosphoproteomes between rice and Arabidopsis (*Arabidopsis thaliana*) using a novel phosphorylation-site evaluation method	*Arabidopsis thaliana* cell suspensions line (ecotype Landsberg erecta) grown at 22 °C in MS medium adjusted at pH 5.7, containing sucrose 3% (w/v), MES 3 mM, myoinositol 100 mg.L^{-1}, thiamine-HCl 10 mg.L^{-1}, pyridoxine-HCl 1 mg.L^{-1}, nicotinic acid 1 mg.L^{-1}, 1-naphthaleneacetic acid 0.5 mg.L^{-1} and 6-benzylaminopurine 0.05 mg.L^{-1}	16 h light/8 h dark
22438062	To gain insights into adaptive processes to low Fe availability at the posttranslational level using a quantitative analysis of Fe deficiency-induced changes in the phosphoproteome profile of Arabidopsis (*Arabidopsis thaliana*) roots	*Arabidopsis thaliana* (ecotype Columbia-0) seeds were kept for 1 day at 4 °C on Petri dishes in the dark, and transferred to a growth chamber and grown at 21 °C under continuous illumination (50 µmol.m^{-2}.s^{-1}; Phillips TL lamps). The growth medium was made of : KNO_3 (5 mM), $MgSO_4$ (2 mM), Ca $(NO_3)_2$ (2 mM), KH_2PO_4 (2.5 mM); H_3BO_3 (70 µM), $MnCl_2$ (14 µM), $ZnSO_4$ (1 µM), $CuSO_4$ (0.5 µM), NaCl (10 µM), Na_2MoO_4 (0.2 µM), and FeEDTA (40 µM), solidified with Phytagel (Sigma-Aldrich) (0.3 % w/v). Sucrose (43 mM) and MES (4.7 mM) were included, and the pH was adjusted to 5.5. After 10 days of precultivation, plants were transferred to fresh agar medium either with FeEDTA (40 µM; +Fe plants) or without Fe and with 3-(2-pyridyl)-5,6-diphenyl-1,2,4-triazine sulfonate (100 µM; ferrozine; −Fe plants) to trap residual Fe. Plants were grown for 3 days on Fe-free medium before analysis. Phosphate deficiency was applied by growing plants on phosphate-free medium for 3 days	continuous light of 50 µmol.m^{-2}.s^{-1}
22329444	To better understand the molecular mechanisms of plant N responses, using two-dimensional gel-based proteomic and phosphoproteomic approaches to profile the proteins with abundance and phosphorylation state changes during nitrate deprivation and recovery in the model plant *Arabidopsis thaliana*	*Arabidopsis thaliana* (ecotype Columbia-0) seeds were cold-treated at 4 °C for 2 days and germinated seeds were grown around flasks and temperature at 22 °C in an Innova 4340 illuminated shaker (New Brunswick Scientific) at a speed of 90 rpm. After 7 days, the media were changed in all flasks; some received 1/2 MS (+N) media 100 mL as the control while others received N free (−N) media (no KNO_3, which was replaced by KCl 5 mM for N deprivation. On day 8 (24 h after N deprivation), the media were renewed in all flasks. On day 9 (48 h after N deprivation), the media in some of the −N flasks were changed into +N media for recovery and the media in other flasks were renewed with N-free media	continuous light of 50 µmol.s^{-1}.m^{-2}
23172892	To identify and quantify, with high selectivity, site-specific phosphorylation of MPK substrate candidates in the model plant *Arabidopsis thaliana*	*Arabidopsis thaliana* seedlings GVG::FLAG-NtMEK2DD grown in 50 mL 1/2 MS medium at 22 °C in continuous light (70 µmol.s^{-1}.m^{-2}). Twelve-day-old seedlings were treated with DEX (1 µM) in ethanol or with ethanol as a control and collected 6 h after treatment	continuous light of 70 µmol.s^{-1}.m^{-2}
23572148	To identify multiple components of the ABA-responsive protein phosphorylation network using the SnRK2 triple mutant	*Arabidopsis thaliana* (ecotype Columbia-0) and *srk2dei* seeds were sown on germination medium agar plates. After stratification for days at 4 °C, the plates were placed at 22 °C under 16 h light/8 h dark conditions for 2 weeks. After preconditioning plants in water (10 mL) in a plastic plate overnight, 30 to 40 plants were exposed to ABA treatment or dehydration stress as follows. For ABA treatment, plants were placed in (±)-ABA (10 mL of 50 µM) for 0, 15, 30, and 90 min. For dehydration stress, plants were placed on plastic plate without any solution for 0, 15, 30, and 90 min. Plant samples were frozen in liquid nitrogen and stored at −80 °C	16 h light/8 h dark
23111157	To better understand the phosphorylation regulatory network in plants	*Arabidopsis thaliana* (ecotype Columbia-0) seedlings hydroponically grown. Briefly, sterilized Arabidopsis seeds were imbibed in sterile half-strength MS medium containing MS Vitamin Mixture (Caisson labs, USA), sucrose (0.5 %), MES (3 mM), pH 5.7 at a ratio of 10 mg of seeds/100 mL of media. Seeds were cold-treated at 4 °C for 2 days and grown under continuous light of 50 µmol.s^{-1}.m^{-2} at 22 °C in an Innova 4340 illuminated shaker (New Brunswick Scientific) at a 90 rpm speed. After 7 days, the media in all flasks were refreshed and after another 2 days, the whole seedlings were harvested and immediately frozen in liquid nitrogen	continuous light of 50 µmol.s^{-1}.m^{-2}
23776212	To identify additional substrate proteins of the SnRK2s and provide insight into the molecular actions of ABA using quantitative phosphoproteomics to compare the global changes in phosphopeptides in WT and snrk2.2/2.3/2.6 triple mutant seedlings in response to ABA treatment.	*Arabidopsis thaliana* seedlings were grown in half-strength MS medium (40 mL) at 22 °C in continuous light on a rotary shaker set at 100 rpm. Twelve-day-old seedlings were treated with ABA in ethanol (50 µM) or with ethanol as the control for 30 min	continuous light
23660473	To measure phosphoproteome responses to osmotic stress in Arabidopsis with a novel mass spectrometry-based label-free quantitation method that facilitates systematic profiling plant phosphoproteome changes with high efficiency and accuracy	*Arabidopsis thaliana* (ecotype Columbia-0) seeds were grown in liquid medium (1/2 MS salts and sucrose (1.5 % w/v)) with 24 h light at room temperature with shaking at 30 rpm. For the osmotic stress treatment, seedlings of 12-day-old were transferred to fresh medium or medium containing mannitol 800 mM for 30 min. For the ABA treatment, the 12-day-old seedlings were transferred to fresh medium containing ABA 100 µM for 30 min	continuous light
24043427	To address how ethylene alters the cellular protein phosphorylation profile in a time-dependent manner	*Arabidopsis thaliana* (ecotypes Columbia-0 and *ctr1-1* mutant) were mixed with agar solution (0.1 % (w/v)) and sown on agar growth media containing KNO_3 (9 mM), $Ca_3OH(PO_4)_3$ (0.4 mM), $MgSO_4$ (2 mM), H_3PO_4 (1.3 mM), Fe-EDTA 50 µM, H_3BO_3 (70 µM), $MnCl_2$ (14 µM), $CuSO_4$ (0.5 µM), $ZnSO_4$ (1 µM), Na_2MoO_4 (0.2 µM), NaCl (10 µM), $CoCl_2$ (0.01 µM), sucrose (10 g.L^{-1}), thiamine-HCl (1 mg.L^{-1}), pyridoxine (0.1 mg.L^{-1}), nicotinic acid (0.1 mg.L^{-1}), myo-inositol (100 mg.L^{-1}), and bacteriological agar (0.8 % w/v, pH 5.7). In each growth jar, 13 to 16 rcn1-1 seeds or 18 to 24 of both ACC-treated wild-type and *ctr1-1* seeds were sown. Seeds for the normal size plant were sown about 1.5 to 2 cm apart from each other, and dwarf plants were sown 1 to 1.5 cm apart. In each biological replicate, 10 to 20 jars of Arabidopsis plants were routinely grown for each treated or unique genotype plant group. These jars were then transferred to plant growth chambers with a 16 h light/8 h dark cycle with a constant temperature of 22 °C ± 2 °C	16 h light/8 h dark
23328941	To identify and quantify the early signaling events following lateral root auxin-inducible system using combined (15)N-based metabolic labeling and phosphopeptide enrichment and applied a mass spectrometry-based approach	*Arabidopsis thaliana* (ecotype Columbia-0) seeds were liquid-sterilized and sown on agar (0.6 %) in a hydroponic system supplied with single component B5 medium containing [^{14}N] or [^{15}N] ammonium nitrate and potassium nitrate. Seeds were vernalized for 2 days at 4 °C in the darkness and transferred to long day growth conditions (16 h light/8 h dark)	16 h light/8 h dark
24601666	To obtain high confidence substrate phosphorylation sites and assign them to specific kinases and to search for rapidly phosphorylated proteins in *Arabidopsis thaliana* in response to bacterial flagellin, a pathogen-associated molecular pattern (PAMP)	*Arabidopsis thaliana* (ecotype Columbia-0) seeds were surface sterilized and stratified for several days at 4 °C. Seedlings were first grown for 5 days in liquid 1/2 MS medium (M6899, Sigma-Aldrich) containing MES (0.5 g.L^{-1}) (M8250, Sigma-Aldrich) pH 5.7 and sucrose 1 % (w/v) (S5016, Sigma-Aldrich) in a culture chamber at 24 °C with a 16 h photoperiod. Then, seedlings were transferred to Erlenmeyer flasks and grown under shaking in the same medium, in the dark, at 25 °C for about 1 month. Plants are grown in the dark to avoid high ribulose-1,5-bisphosphate carboxylase/oxygenase (RuBisCO) content in the plant tissues as RuBisCO is the most abundant protein in photosynthetic organisms. The culture in liquid medium allowed applying the PAMP flg22 easily and on a large plant surface.	continuous dark during 1 month
25561503	To study DNA damage repair in *Arabidopsis thaliana* using mass spectrometry-based phosphoproteomics approach	*Arabidopsis thaliana* wild type plants (ecotype Columbia-0) and mutant lines (double homozygous offspring of a double heterozygous *atm atr* line were grown side-by-side under long day conditions (16 h light, 8 h dark, 21 °C; 60 to 80 % humidity, 5800 LUX, 3× Philips TLD 36W, and 2× Sylvana GroLUX 36W). For irradiation experiments, plants were exposed to 100 Gy ionizing radiation using a Co60 source (25 Gy min^{-1}). For each sample, the aerial parts of three plants were harvested 15 min after irradiation. Samples were pooled, frozen in liquid nitrogen, and stored at −80 °C	16 h light/8 h dark
26091701	To better elucidate post-translational events tied to the circadian system in Arabidopsis seedlings	*Arabidopsis thaliana* (ecotype Clumbia-0) seedlings were entrained under 12 h white fluorescent light (120 µmol.s^{-1}.m^{-2})/12 h dark cycles for 10 days on MS medium plates with sucrose 3 % w/v and agar 1 % w/v at 22 °C. The seedlings were then maintained under constant light and temperature for 24 h before harvesting. The tissues were harvested in tubes containing Zirconia beads at serveral time points during the 12th day of growth and frozen immediately	12 h light 120 µmol.s^{-1}.m^{-2} /12 h dark cycles for 10 days and constant light for 24 h
26187819	To conduct a global and dynamic phosphoproteome profiling across five time points of brassinosteroid treatment in the period between 5 min and 12 h	*Arabidopsis thaliana* (ecotype Landsberg erecta) cell suspension cultures maintained in MS medium (50 mL) (4.43 g.L^{-1}), sucrose (30 g.L^{-1}), naphthalene acetic acid (0. mg.L^{-1}), kinetin (0.05 mg.L^{-1}); adjusted to pH 5.7 with KOH (1 M) at 27 °C under gentle agitation (130 rpm) in the dark. Cells were weekly subcultured in fresh medium at a 1/10 dilutions	continuous dark
29167316	To identify substrates of MAPKs likely involved in cell division, growth and development the phosphoproteomes of wild-type and mpk3, mpk4, and mpk6 were compared. To study the function of these MAPKs in innate immunity, their phosphoproteomes were analyzed following microbe-associated molecular pattern (MAMP) treatment	*Arabidopsis thaliana* (ecotype Columbia-0) was used as wild-type (WT) plant and mpk3–1 (SALK_151594), mpk4–2 (SALK_056245), and mpk6–2 (SALK_073907) as mutants were all grown, treated and harvested as described in Rayapuram *et al.* (2014), previously described in this table	continuous dark during 1 month

Supplementary Table 2. Metabolite levels from light- and light/dark-treated Arabidopsis rosette leaves

	Metabolite name	Light to Light/Dark ratio	Light	Light/Dark	p-value
	2-hydroxyglutaric acid	0,59	0,03 ± 0,01	0,05 ± 0,02	0,14
**	alanine	0,27	42,66 ± 9,87	158,68 ± 6,83	0,00
*	arabinose	0,79	0,38 ± 0,02	0,48 ± 0,04	0,03
*	ascorbic acid	0,70	15,35 ± 1,93	21,87 ± 2,65	0,03
	asparagine	0,29	0,08 ± 0,01	0,28 ± 0,18	0,20
*	aspartic acid	0,40	3,30 ± 0,32	8,14 ± 2,04	0,05
**	β alanine	0,63	0,42 ± 0,07	0,66 ± 0,05	0,01
	benzoic acid	1,10	0,39 ± 0,04	0,35 ± 0,02	0,29
	citramalic acid	0,67	0,12 ± 0,03	0,18 ± 0,03	0,08
**	citric acid	0,45	0,45 ± 0,14	0,99 ± 0,08	0,01
*	cysteine	0,53	0,06 ± 0,01	0,10 ± 0,02	0,05
	di-galactosylglycerol	1,09	0,16 ± 0,02	0,14 ± 0,03	0,56
	ethanolamine	0,89	39,88 ± 4,16	44,67 ± 3,09	0,19
	fructose	2,68	1,71 ± 0,71	0,64 ± 0,17	0,12
	fumaric acid	0,50	75,57 ± 48,46	150,31 ± 28,81	0,10
**	gamma-aminobutyric acid	0,52	0,35 ± 0,04	0,67 ± 0,05	0,00
	galactinol	0,98	0,55 ± 0,07	0,56 ± 0,07	0,83
	galactonic acid	0,85	0,18 ± 0,02	0,21 ± 0,01	0,15
	galactono-1,4-lactone	1,36	1,92 ± 0,67	1,41 ± 0,18	0,32
*	galactose	0,65	0,32 ± 0,07	0,50 ± 0,01	0,05
	galactosylglycerol	0,66	0,26 ± 0,16	0,40 ± 0,13	0,33
	glutamine	0,20	2,15 ± 0,83	10,99 ± 8,05	0,20
**	5-oxopyrrolidine 2-carboxyamide	0,25	0,90 ± 0,33	3,67 ± 0,75	0,01
*	glutamic acid	0,36	2,93 ± 0,12	8,22 ± 1,36	0,02
*	glucose	1,90	1,76 ± 0,35	0,92 ± 0,20	0,03
	glycine	0,80	3,27 ± 1,36	4,07 ± 0,56	0,42
**	glyceric acid	6,00	2,34 ± 0,38	0,39 ± 0,02	0,01
*	glycolic acid	1,46	0,19 ± 0,02	0,13 ± 0,03	0,05
	homoserine	1,34	0,16 ± 0,03	0,12 ± 0,01	0,16
**	isoleucine	0,67	0,92 ± 0,11	1,39 ± 0,02	0,01
	lactic acid	0,74	3,06 ± 1,28	4,11 ± 2,42	0,55
*	lauric acid	5,05	1,03 ± 0,22	0,20 ± 0,01	0,02
	leucine	1,19	0,43 ± 0,14	0,36 ± 0,09	0,53
	linolenic acid	1,01	0,07 ± 0,01	0,06 ± 0,03	0,98
**	lysine	0,47	0,17 ± 0,00	0,36 ± 0,01	0,00
*	malic acid	0,71	2,03 ± 0,33	2,85 ± 0,01	0,05
	mannose	1,06	0,05 ± 0,02	0,05 ± 0,02	0,84
	methionine	1,16	0,09 ± 0,01	0,08 ± 0,01	0,23
	myo-inositol	0,63	3,46 ± 0,11	5,48 ± 1,08	0,08
**	*o*-acetyl-L-serine	0,40	0,07 ± 0,00	0,18 ± 0,01	0,00
	octanoic acid	1,07	0,17 ± 0,03	0,16 ± 0,00	0,57
**	ornithine	2,01	1,06 ± 0,11	0,53 ± 0,10	0,00
*	palmitic acid	2,06	9,09 ± 1,38	4,41 ± 0,21	0,03
	phenylalanine	1,34	0,36 ± 0,07	0,27 ± 0,02	0,16
*	phosphoric acid	0,54	1,15 ± 0,31	2,12 ± 0,42	0,04
**	pipecolic acid	0,45	0,29 ± 0,08	0,64 ± 0,09	0,01
*	proline	1,28	16,08 ± 1,12	12,52 ± 1,48	0,03
	putrescine	0,77	1,50 ± 0,87	1,94 ± 0,11	0,47
*	pyroglutamic acid	0,37	0,47 ± 0,01	1,26 ± 0,21	0,02
	pyruvic acid	0,80	0,76 ± 0,13	0,96 ± 0,05	0,10
*	ribose	0,73	0,36 ± 0,04	0,48 ± 0,04	0,02
	serine	0,71	8,56 ± 2,25	12,07 ± 0,53	0,11
	shikimic acid	0,80	1,03 ± 0,22	1,28 ± 0,12	0,18
**	sinapinic acid	0,48	0,27 ± 0,07	0,57 ± 0,02	0,01
	sorbitol	1,17	12,29 ± 2,73	10,48 ± 0,66	0,37
**	spermidine	0,23	0,05 ± 0,00	0,21 ± 0,02	0,00
*	stearic acid	4,22	16,68 ± 3,13	3,96 ± 0,42	0,02
**	succinic acid	0,28	0,51 ± 0,14	1,84 ± 0,26	0,00
	sucrose	1,44	5,21 ± 1,26	3,62 ± 0,09	0,16
*	tetradecanoic acid	0,92	0,54 ± 0,01	0,58 ± 0,02	0,02
	threonine	0,95	5,45 ± 0,42	5,74 ± 0,17	0,35
*	threitol	0,90	0,26 ± 0,01	0,28 ± 0,01	0,02
**	threonic acid-1,4-lactone	0,66	0,52 ± 0,04	0,79 ± 0,06	0,00
	tyrosine	0,89	0,12 ± 0,01	0,13 ± 0,01	0,11
	tyramine	0,58	0,25 ± 0,02	0,43 ± 0,14	0,15
	urea	0,77	1,39 ± 0,25	1,80 ± 0,91	0,52
	valine	0,85	3,68 ± 0,57	4,31 ± 0,39	0,20
	xylose	0,80	0,71 ± 0,11	0,89 ± 0,08	0,08

Values are mean ± SD metabolite levels (arbitrary units per g DW) from n=3 independent biological replicates of light- and light/dark-treated Arabidopsis plants. Asterisks correspond to significant differences between the two treatments with the following p-values: **≤0.01, * ≤0.05, (2-tailed Student's *t*-test).

Supplementary Table S3: List of the primers used for the cloning and site directed mutagenesis with the corresponding names, sequences and Tm °C.

Aim	primer name	sequence 5'>3'	Tm °C
*At*iPGAM2-WT Cloning into pET16b	pET16b-fw	CTCGAGGATCCGGCTGCTAA	61.4
	pET16b-rev	CTCCATATGACGACCTTCGA	57.3
	iPGAM2-rev16b	TTAGCAGCCGGATCCTCGAGTCACTTCTCGACGACTTCGATC	76.3
	iPGAM2-fw16b	TCGAAGGTCGTCATATGGAGGGTAGCTCCGGCGACGTT	75.9
*At*iPGAM2-S82A Cloning into pET16b	iPGAM2S82Afwd	GGGAAACagTGAAGTTGGCCACAATGCTCTTGG	70.7
	iPGAM2S82Arev	CAACTTCActGTTTCCCATGTCGTCTTCGCTG	69.5
AtiPGAM2-S82D Cloning into pET16b	iPGAM2S82Dfwd	GGGAAACGATGAAGTTGGCCACAATGCTCTTGG	70.7
	iPGAM2S82Drev	CAACTTCATCGTTTCCCATGTCGTCTTCGCTG	69.5
D29N mutagenesis	563PRO	CTATCGGTTTGATTGTTCTCaATGGATGGGGTGAATCTGATCC	72.3
	564TER	GGATCAGATTCACCCCATCCATtGAGAACAATCAAACCGATAG	72.3
R290L mutagenesis	565PRO	CATTCAATTTCCGTGCTGATCttATGGTCATGCATGCAAAGGC	72.3
	566TER	GCCTTTGCATGCATGACCATaaGATCAGCACGGAAATTGAATG	72.3